previously.[3,4] Colony PCR to examine the expression of *Bmi1*, *Ink4a*, and *Arf* was also performed.[9]

Western Blotting

Cells transduced with the indicated retroviruses were selected by cell sorting for EGFP expression and subjected to Western blot analysis using anti-Bmi1 (F6; Upstate Biotechnology), anti-β-catenin (clone14; BD), anti-cyclin D1 (DCS-6; BD), anti-c-Myc (9E10; Santa Cruz Biotechnology, Santa Cruz, CA) or antitubulin (Ab-1; Oncogene Science, Cambridge, MA) antibodies.

Luciferase Assay

pTOPFLASH or pFOPFLASH (Upstate Biotechnology) was used to determine the transcriptional activation or suppression of the Tcf-reporter plasmid. Luciferase assays were performed using the Dual Luciferase Reporter Assay System (Promega, Madison, WI). Relative luciferase activities were calculated as the ratio of pTOPFLASH to pFOPFLASH.

Cell-Cycle Analysis

Cells transduced with the indicated retroviruses were fixed with 70% ethanol in phosphate-buffered saline and stained with 50 μg/mL of propidium iodide. Cell-cycle analyses were performed on a FACSCalibur (BD).

Anchorage-Independent Colony Formation Assay

A total of 5×10^4 cells originating from H-CFU-Cs transduced with the indicated retroviruses were sus-

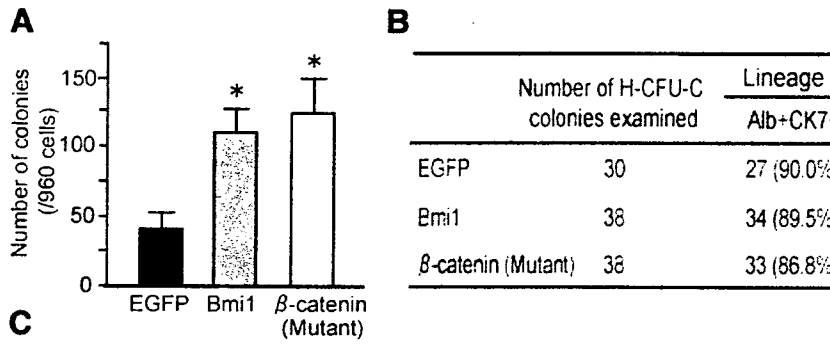

B

	Number of H-CFU-C colonies examined	Lineage marker of cells in a H-CFU-C colony			
		Alb+CK7+	Alb+CK7-	Alb-CK7+	Alb-CK7-
EGFP	30	27 (90.0%)	0	2 (6.7%)	1 (3.3%)
Bmi1	38	34 (89.5%)	0	3 (7.9%)	1 (2.6%)
β-catenin (Mutant)	38	33 (86.8%)	0	4 (10.5%)	1 (2.6%)

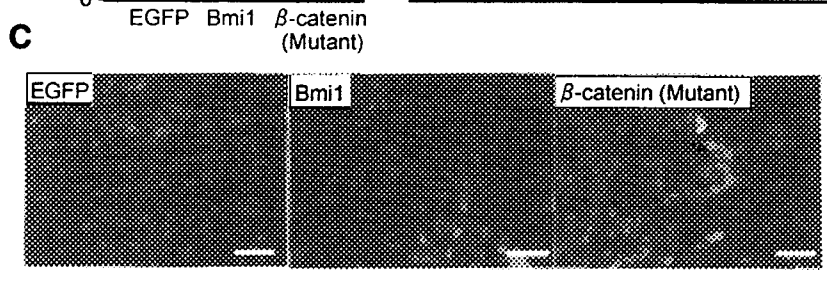

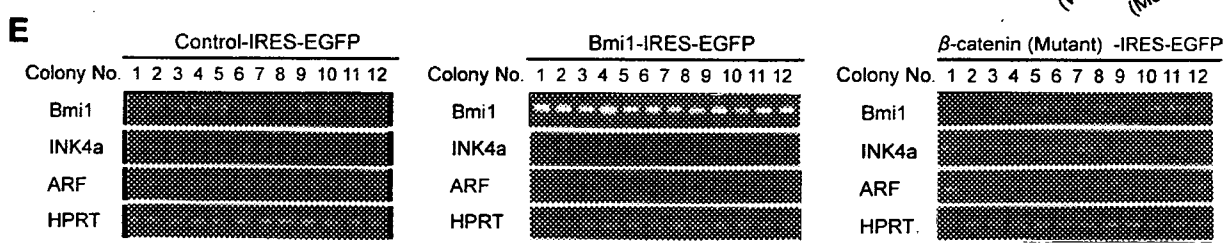

Figure 4. Effects of forced expression of *Bmi1* and constitutively active *β-catenin*. (*A*) Single colonies at day 42 in Figure 1E were clonally sorted into microtiter plates, and the number of secondary colonies generated per 960 clone-sorted cells were counted. The number of colonies derived from single primary colonies expressing EGFP, Bmi1, and mutant β-catenin was 39.4 ± 9.6, 108.5 ± 16.9, and 122.0 ± 27.4, respectively. These results are representative of 3 independent experiments (scale bar, 50 μm). *Statistically significant ($P < .05$). (*B*) Immunocytochemical analyses of secondary colonies generated in Figure 4A revealed that >85% of colonies consisted of bilineage cells. (*C*) An increase in the number of bipotent cells (*yellow*) expressing both albumin (*red*) and CK7 (*green*) was observed in secondary colonies expressing Bmi1 or active β-catenin compared with the control (scale bar, 50 μm). (*D*) TOP/FOP luciferase reporter assays showed that the Tcf-reporter activity in H-CFU-C colonies was increased by transduction of mutant *β-catenin*, but not of *Bmi1*. The TOP-to-FOP ratio in cells derived from H-CFU-Cs transduced with *EGFP*, *Bmi1*, wild-type *β-catenin*, and mutant *β-catenin* was 1.2 ± 0.2, 1.1 ± 0.3, 1.7 ± 0.4, and 6.9 ± 1.4, respectively. *Statistically significant ($P < .05$). (*E*) Colony PCR showed that transduction of *Bmi1* repressed the expression of $p16^{Ink4a}$ and $p19^{Arf}$. In contrast, colonies derived from H-CFU-Cs transduced with mutant β-catenin showed neither up-regulation of Bmi1 nor down-regulation of $p16^{Ink4a}$ and $p19^{Arf}$.

pended in 2.0 mL of 0.3% agar (Wako, Osaka, Japan) supplemented with the culture medium. The cell suspension was layered over the bottom layer of 2.0 mL of 0.6% agar. Colonies >100 μm in diameter were counted in triplicate dishes at day 21 of culture.

Transplantation of Transduced Cells and Histologic Analysis

A total of 2 × 10^6 cells derived from H-CFU-Cs transduced with the indicated retroviruses were suspended in *Dulbecco* Modified Eagle Medium/F-12 and Matrigel (BD) (1:1) and injected into the subcutaneous space of NOD/SCID mice (8–10 weeks old) under anesthesia, and tumor formation was monitored weekly for 18 weeks. The cells were also transplanted into the spleen of mice that had undergone a partial hepatectomy with pretreatment with 20 mg/kg 2-acetylaminofluorene (AAF) for 5 days as described previously.[28,29] Paraffin-embedded sections or frozen sections of murine tumors were stained with H&E. They were also stained with anti-EGFP (BD Biosciences Clontech, Palo Alto, CA), antialbumin, and anti-CK7 as described previously.

Statistics

Data represent means ± SEMs. Statistical differences between groups were analyzed using the Mann-Whitney *U* test. Differences were considered significant at $P < .05$.

Results

Basal Expression and Propagation Effect of Bmi1 or β-catenin in Hepatic Stem/Progenitor Cells

To evaluate the role of Bmi1 and β-catenin in hepatic stem/progenitor cells, $CD45^-Ter\text{-}119^-$ cells were further fractionated into 4 subpopulations as follows: $CD29^-CD49f^-$ cells (fraction 1), $CD29^+CD49f^-$ cells

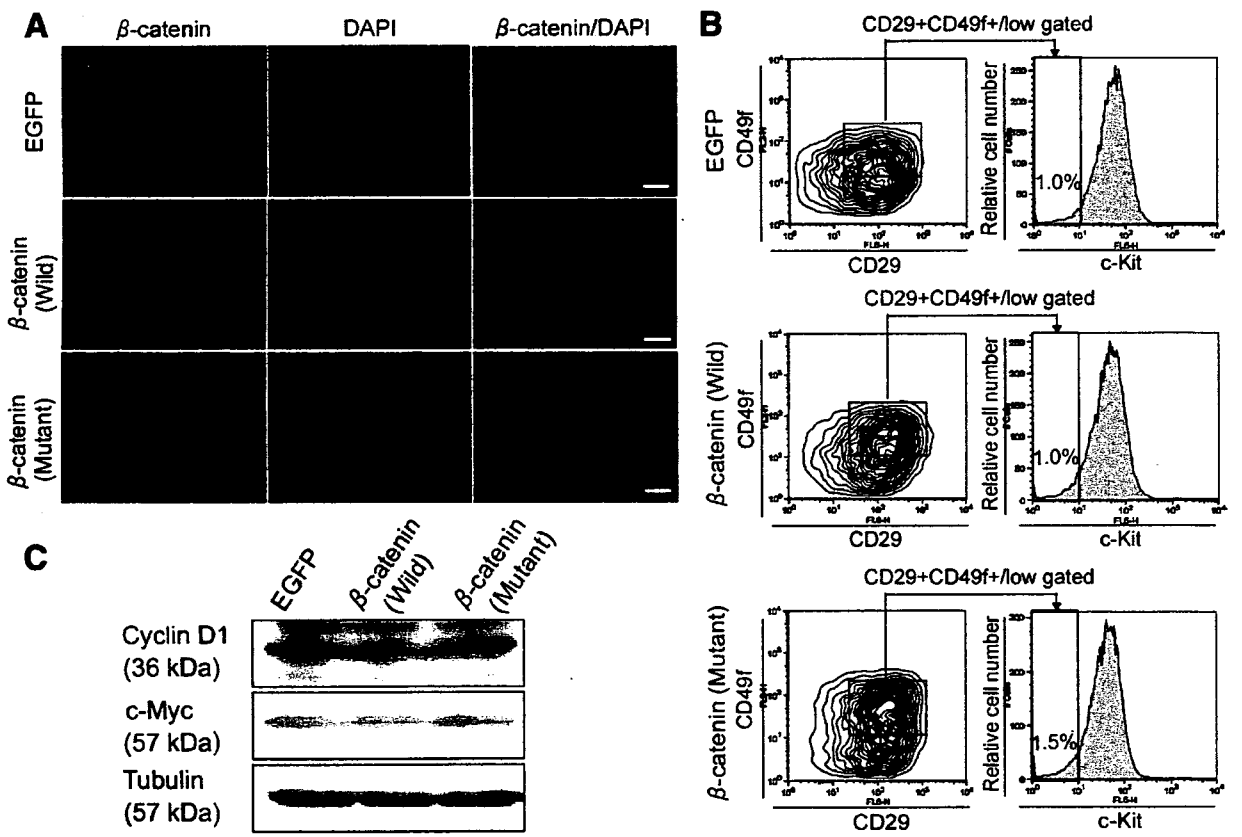

Figure 5. Characterization of colonies derived from H-CFU-Cs transduced with wild-type *β-catenin* or mutant *β-catenin* at day 14 of culture. (*A*) Immunocytochemical analyses showed that β-catenin was located in close proximity to the cell membrane in the control colonies. In addition, a cytoplasmic distribution of β-catenin was also found in colonies expressing wild-type β-catenin. Moreover, both the cytoplasmic and nuclear localization of β-catenin was observed in colonies expressing mutant β-catenin (scale bar, 50 μm). (*B*) The percentage of $c\text{-}Kit^-CD29^+CD49f^{+/low}$ $CD45^-Ter\text{-}119^-$ cells in H-CFU-C colonies transduced with *EGFP*, wild-type *β-catenin*, and mutant *β-catenin* at day 14 of culture was 0.9% ± 0.2%, 1.0% ± 0.2%, and 1.4% ± 0.4%, respectively. (*C*) Western blotting revealed that transduction of neither wild-type *β-catenin* nor mutant *β-catenin* induce up-regulation of cyclin D1 and c-Myc.

(fraction 2), c-Kit$^+$CD29$^+$CD49f$^{+/low}$ cells (fraction 3), and c-Kit$^-$CD29$^+$CD49f$^{+/low}$ cells (fraction 4) (Figure 1*A*). Real-time RT-PCR showed the expression of *Bmi1* and *β-catenin* to be significantly increased in fraction 4 compared with the other 3 fractions (Figure 1*B*). Immunocytochemical analyses confirmed that Bmi1 is expressed in the nucleus of most of the fraction 4 cells. In contrast, nuclear/cytoplasmic expression of β-catenin in approximately 60% of fraction 4 cells suggested limited activation of Wnt/β-catenin signaling in these cells (Figure 1*C*). Fraction 4, which represented approximately 2.0% of all fetal liver cells, was rich in H-CFU-Cs, whereas the other 3 fractions (fractions 1–3) barely contained H-CFU-Cs (Figure 1*A*). Furthermore, the most primitive H-CFU-Cs that kept growing and gave rise to large colonies were exclusively present in fraction 4. To obtain new insight into the self-renewal mechanisms of hepatic stem cells, we conducted gain-of-function assays by overexpressing either *Bmi1* or constitutively active *β-catenin*. Retroviral manipulation showed no significant differences in the frequency of colony formation at days 5 and 42 in culture (Figure 1*D*). However, H-CFU-Cs expressing Bmi1 or mutant β-catenin showed promoted proliferation and gave rise to significantly larger colonies at day 42 than did those of the control expressing EGFP (Figure 1*E* and *F*). Notably, these colonies exhibited a "pile-up" appearance in the central areas, indicating anchorage-independent growth (Figure 1*E*) and were composed of a larger number of cells than were the control (Figure 1*G*). In contrast, the colonies derived from H-CFU-Cs transduced with wild-type *β-catenin* showed no morphologic changes (data not shown). However, the other 3 fractions (fractions 1–3) failed to form colonies during 14 days irrespective of the transduction of *Bmi1* or mutant *β-catenin* (Figure 1*D*).

Enhancement of Self-Renewal Capability in Hepatic Stem/Progenitor Cells Transduced With Bmi1 or Mutant β-catenin

The colonies at day 42 in the control, Bmi1, wild-type β-catenin, and mutant β-catenin cultures were subcultured. FACS and Western blot analysis showed that most cells expressed EGFP, a marker for retrovirus integration (Figure 2*A*). The expression of each gene was verified by Western blot analysis (Figure 2*B* and *C*). The secondary colonies generated exhibited similar characteristics to each primary colony in terms of colony size and morphologic features (Figure 3).

We then clonally replated the colonies at day 42 into 960 microtiter wells to evaluate the content of H-CFU-Cs in the primary colonies. The H-CFU-C frequencies in the primary colonies were increased roughly 2.7- and 3.0-fold by the forced expression of *Bmi1* and mutant *β-catenin*, respectively (Figure 4*A*). Immunocytochemical analyses on single secondary colonies using a hepatocyte-specific marker, albumin, and a cholangiocyte-specific marker, CK7, indicated that >85% of colonies derived from clone-sorted H-CFU-Cs transduced with the viruses consisted of both albumin$^+$ cells and CK7$^+$ cells at day 14 of culture (Figure 4*B*). The results of colony PCR for hepatocyte and cholangiocyte lineage markers also showed that the H-CFU-Cs overexpressing Bmi1 or mutant β-catenin retain bipotent differentiation potential (Supplementary Table 1; see supplemental material online at www.gastrojournal.org). Forced expression of *Bmi1* or

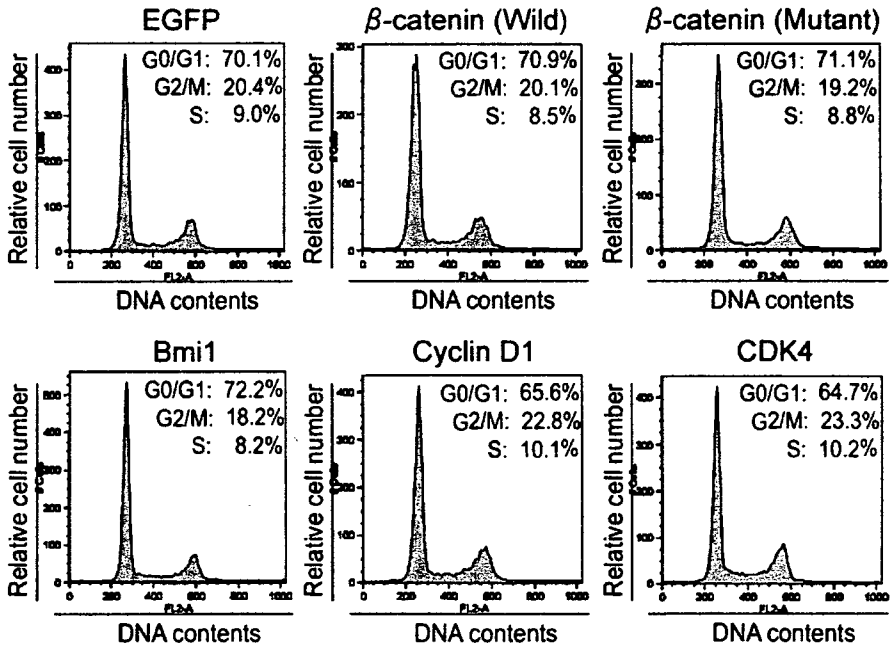

Figure 6. Representative FACS analyses of the cell cycle. Although transduction of cell-cycle regulators, *cyclin D1* and *CDK4*, promoted cell-cycle entry and increased cell numbers in S and G_2/M phases, H-CFU-C colonies expressing β-catenin or Bmi1 showed a similar pattern to the control.

mutant *β-catenin* led to an increase in the proportion of albumin$^+$CK7$^+$ cells, which are putative bipotential progenitor cells, compared with the control (Figure 4*C*). Given that the cell numbers comprising the primary colonies were 4.9- and 5.6-fold larger on *Bmi1* and mutant *β-catenin* transduction, respectively (Figure 1*G*), forced expression of *Bmi1* and mutant *β-catenin* achieved 12.3- and 16.4-fold expansion of bipotent H-CFU-Cs during the initial 42-day culture, respectively. These results indicate that forced expression of Bmi1 or mutant β-catenin enhances self-renewal of hepatic stem/progenitor cells in culture without affecting the bilineage differentiation potential of the transduced hepatic stem/progenitor cells.

We were then interested in the relation between Bmi1 and the Wnt/β-catenin signal as self-renewal regulators of hepatic stem/progenitor cells. The TOP/FOP luciferase assay revealed that the introduction of mutant *β-catenin* actually activated the canonical Wnt/β-catenin pathway, whereas that of wild-type *β-catenin* or *Bmi1* did not (Figure 4*D*). Conversely, colony PCR showed that the introduction of mutant *β-catenin* did not augment *Bmi1* expression (Figure 4*E*). As reported,[30] *Bmi1* overexpression repressed the expression of $p16^{Ink4a}$ and $p19^{Arf}$, whereas the expression of mutant *β-catenin* had no effect. These results indicate that Bmi1 and the Wnt/β-catenin pathway independently regulate the self-renewal of hepatic stem/progenitor cells.

Effects of Wnt/β-catenin Signaling on Stemness Features

To clarify the functional significance of the Wnt/β-catenin signaling, we first analyzed the subcellular distribution of β-catenin in H-CFU-C colonies expressing EGFP, wild-type β-catenin, or mutant β-catenin. Immunocytochemical analyses revealed that β-catenin was located in close proximity to the cell membrane in all cells analyzed. In β-catenin–transduced cells, it also distributed in the cytoplasm. As expected, however, it was detected in the nucleus only in the cells expressing mutant β-catenin (Figure 5*A*). Next, to address whether the Wnt/β-catenin pathway is relevant to the maintenance of stem/progenitor cells, FACS analyses of the colonies derived from H-CFU-Cs transduced with indicated viruses were performed. The percentages of c-Kit$^-$CD29$^+$CD49f$^{+/low}$CD45$^-$Ter-119$^-$ cells showed a slight increase in colonies derived from H-CFU-Cs expressing mutant β-catenin compared with those from H-CFU-Cs expressing EGFP or wild-type β-catenin (Figure 5*B*). Although we estimated the expression levels of cyclin D1 and c-Myc, well-known downstream targets of Wnt/β-catenin signaling,[31,32] introduction of neither wild-type nor mutant *β-catenin* into H-CFU-Cs altered their expression in secondary colonies (Figure 5*C*).

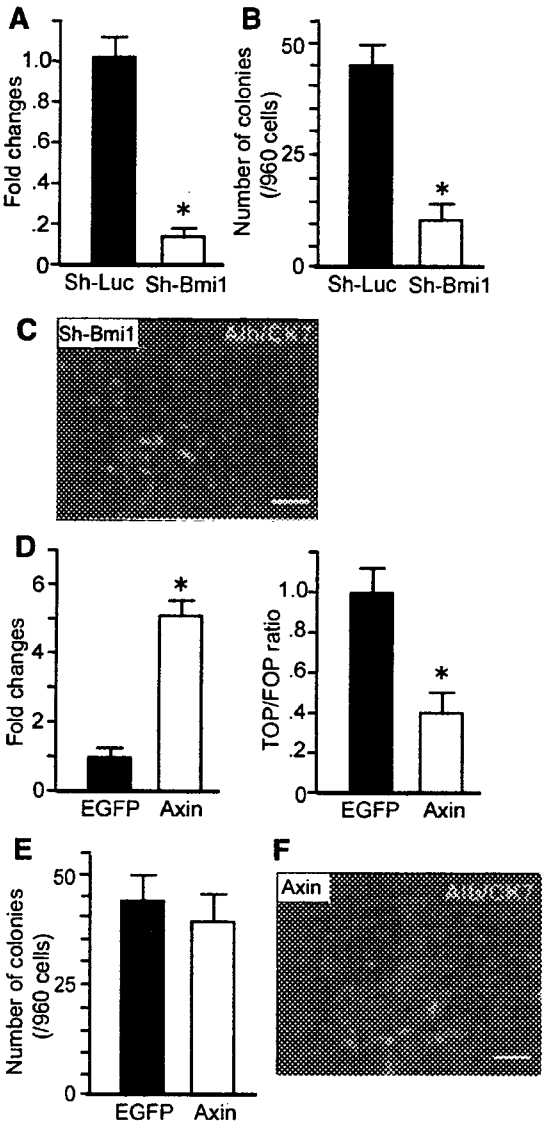

Figure 7. Loss-of-function analysis of Bmi1 and the Wnt/β-catenin pathway. (*A*) Expression of shRNA against *Bmi1* resulted in an approximately 9.0-fold decrease in endogenous mRNA expression of *Bmi1*. Luc indicates luciferase; *statistically significant ($P < .05$). (*B*) Knockdown of *Bmi1* markedly decreased the colony-forming capacity of H-CFU-Cs. The number of H-CFU-C colonies expressing shRNA against *luciferase* and *Bmi1* was 44.2 ± 5.6, and 11.0 ± 4.4, respectively. *Statistically significant ($P < .05$). (*C*) In H-CFU-C colonies expressing shRNA against *Bmi1*, the number of bipotent cells expressing both albumin (*red*) and CK7 (*green*) was also decreased (scale bar, 50 μm). (*D*) Real-time RT-PCR showed a nearly 5.0-fold increase in the mRNA level of *Axin* in transduced cells (*left panel*). TOP/FOP reporter assays also showed the successful repression of the Tcf-reporter activity (*right panel*). *Statistically significant ($P < .05$). (*E*) Transduction of *Axin* did not affect the colony-forming capacity of H-CFU-Cs. The number of H-CFU-C colonies after transduction with *EGFP* or *Axin* was 43.5 ± 6.5 and 38.1 ± 7.8, respectively. (*F*) In H-CFU-C colonies expressing *Axin*, the number of bipotent cells expressing both albumin (*red*) and CK7 (*green*) was maintained, but differentiation was slightly skewed to the albumin$^+$ hepatocyte-lineage (*red*) (scale bar, 50 μm).

Flow Cytometric Analyses of the Cell-Cycle Status

Next, cell-cycle status was analyzed in H-CFU-C colonies transduced with the viruses together with those transduced with *cyclin D1* and *CDK4*, positive regulators of the cell cycle (Figure 6). Transduction of *cyclin D1* or *CDK4* into H-CFU-C colonies showed an increase in number of cells in the S and G_2/M phases compared with the control. However, no significant change was observed in cell-cycle status in the H-CFU-C colonies expressing Bmi1, wild-type β-catenin, or mutant β-catenin. These results indicated that overexpression of Bmi1 or β-catenin does not affect the cell-cycle status of H-CFU-Cs. Thus, as indicated in Figure 5*C*, up-regulation of the expression of cyclin D1, one of the Wnt/β-catenin targets, which leads to promoted G_1/S transition, is supposedly not a key mechanism of the Wnt/β-catenin-mediated biologic effects on H-CFU-Cs.

Essential Role of Bmi1 in Self-Renewal of Hepatic Stem/Progenitor Cells

To elucidate whether Bmi1 and the Wnt/β-catenin pathways are essential for hepatic stem cell self-renewal in culture, we performed loss-of-function assays. Colonies derived from nontransduced H-CFU-Cs were subcultured and transduced with *Axin*, an inhibitor of the Wnt/β-catenin signal or shRNA against *Bmi1*. Subsequently, the colonies were subjected to single-cell culture. Expression of shRNA against *Bmi1* resulted in an approximately 4.0-fold decrease in H-CFU-C numbers (Figure 7*A* and *B*), and the colonies generated were significantly smaller than the control (Figure 7*C*). Immunocytochemical analysis also showed a decrease in the number of albumin$^+$CK7$^+$ putative bipotent progenitor cells (Figure 7*C*). In contrast, although forced expression of *Axin* in H-CFU-Cs significantly suppressed the Wnt/β-catenin signal as evidenced by a decrease in Tcf-reporter activity (Figure 7*D*), it had no significant impact on H-CFU-C numbers (Figure 7*E*), the secondary colony size, or the frequencies of bipotent cells in secondary colonies (Figure 7*F*). However, it somewhat skewed their differentiation into the hepatocyte lineage (Figure 7*F*). This effect of Axin on differentiation is reminiscent of that of β-catenin antisense on embryonic liver cultures.[33]

Neoplastic Transformation of Hepatic Stem/Progenitor Cells in Culture and In Vivo

The "pile-up" appearance of the colonies expressing either Bmi1 or mutant β-catenin (Figure 1*E*) prompted us to examine their anchorage-independent growth in soft agar. In contrast to the control cells, nearly 8% of the cells expressing Bmi1 or mutant β-catenin formed large colonies (Figure 8), indicating promoted transformation of hepatic stem/progenitor cells in culture. To confirm these findings in vivo, we next injected them into NOD/SCID mice (Figure 9*A*). All mice transplanted with cells expressing either Bmi1 or mutant β-catenin exhibited a similar course of tumor development and died with symptoms of cachexia within 18 weeks after the transplantation (Figure 9*C*). Intriguingly,

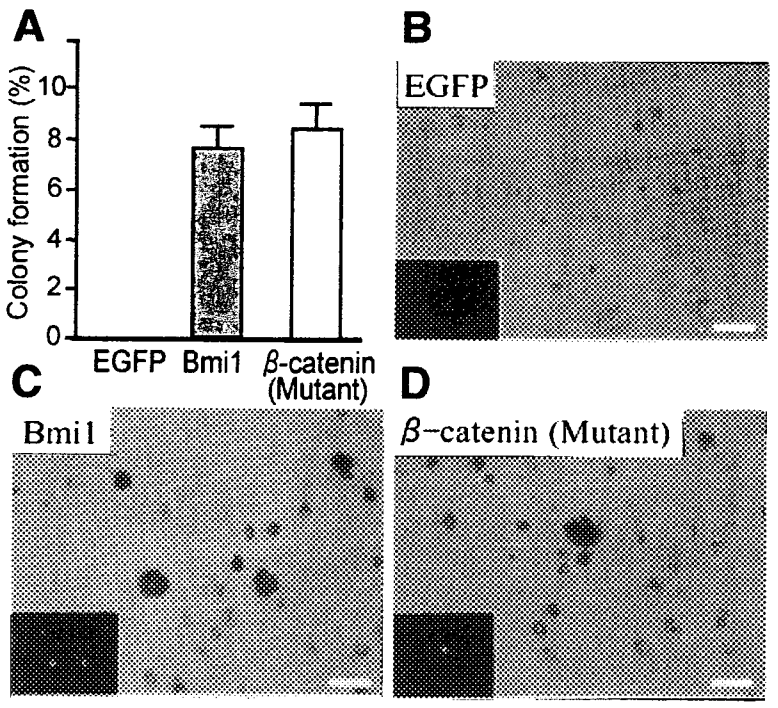

Figure 8. Anchorage-independent colony formation in soft agar. (*A*) The percentage of anchorage-independent colonies >100 μm in diameter after incubation for 21 days, that originated from H-CFU-Cs transduced with *Bmi1* or *mutant β-catenin*, was 7.8 ± 0.6 and 8.1 ± 0.8, respectively. The data represent the mean ± standard deviation of triplicate samples. Scale bar, 100 μm. (*B–D*) Cells originating from H-CFU-Cs transduced with *Bmi1* (*C*) or mutant *β-catenin* (*D*) generated much larger colonies than did the control cells (*B*) (scale bar, 100 μm).

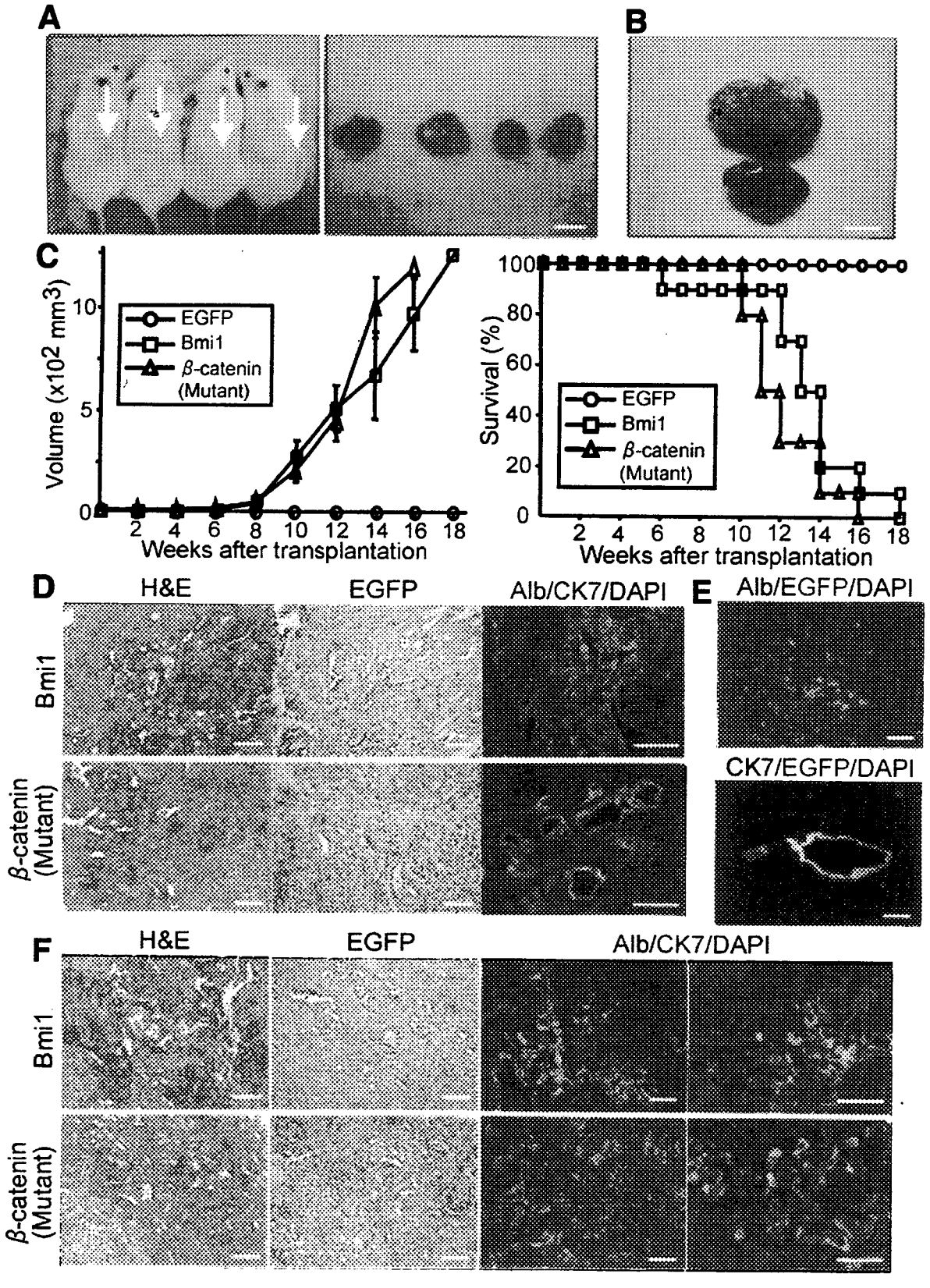
A
B
C
Volume (x10² mm³)
EGFP
Bmi1
β-catenin (Mutant)
Weeks after transplantation
Survival (%)
D
H&E
EGFP
Alb/CK7/DAPI
Bmi1
β-catenin (Mutant)
E
Alb/EGFP/DAPI
CK7/EGFP/DAPI
F

the histologic analysis of tumors derived from both *Bmi1*- and mutant *β-catenin*-transduced H-CFU-Cs revealed nodular proliferation of undifferentiated cells (Figure 9*D*). These cells showed evident nuclear atypia such as nuclear enlargement, irregularities of the nuclear membrane, and nuclear pleomorphism. Immunohistochemical analysis revealed that the tumors consisted of parenchyma composed of albumin$^+$ hepatocytes and glandular structures composed of CK7$^+$ cholangiocytes (Figure 9*D*).

To directly address whether disrupted self-renewal of hepatic stem/progenitor cells contributes to hepatocarcinogenesis, the transduced cells were injected into the spleen of NOD/SCID mice that had received a preconditioning treatment consisting of AAF administration and partial hepatectomy. The transplantation of cells originating from H-CFU-Cs expressing Bmi1 or mutant β-catenin induced marked hepatomegaly with a large number of tumor nodules in recipient livers at 8 weeks after the injection (Figure 9*B*). Control cells expressing EGFP efficiently contributed to the regeneration of recipient livers as evidenced by a large number of EGFP$^+$albumin$^+$ parenchyma cells and EGFP$^+$CK7$^+$ ductlike structures (Figure 9*E*). However, tumor nodules that had originated from H-CFU-Cs transduced with Bmi1 or mutant β-catenin were not encapsulated and had well-defined expansive margins (Figure 9*F*). Unexpectedly, but importantly, these tumors again displayed histopathologic characteristics that mimicked those of subcutaneous tumors. The tumors showed both the proliferation of albumin$^+$ cells and CK7$^+$ ductlike structures corresponding to well-differentiated cholangiocarcinoma (CC). The tumor contained focal areas with hepatocyte-like polygonal cells having an eosinophilic cytoplasm and importantly several small nests of bipotent cells, expressing both albumin and CK7 simultaneously. Spindle-shaped undifferentiated cells with the characteristics of sarcoma were also observed in the tumors originating from *Bmi1*-transduced H-CFU-Cs. The 2 major components of the tumor, HCC and CC, were intimately intermingled and exhibited no clear border, which distinguished the tumor from so called "collision tumor" consisting of HCC and CC. Taken together, these tumors were diagnosed as combined HCC and CC (cHCC-CC).

Discussion

An excessive and persistent self-renewal signal is one of the key events in the initial stages of carcinogenesis.[34] This was clearly shown in the hematopoietic system, in which oncogenic events, including breakpoint cluster region-Abelson oncogene locus translocation and the constitutive activation of signal transducer and activator of transcription 5, enhance the self-renewal of HSCs and establish chronic myeloproliferative disorders.[35,36] It is believed that rare transforming events tend to occur in stem cells because they are the only cells that self-renew throughout life. In fact, there is increasing evidence to support the idea that stem cells and their immediate progeny are the primary targets of transformation.

In terms of hepatocarcinogenesis, it has traditionally been believed that long-term, repeated injury and regeneration of damaged mature cells induce an accumulation of multiple genetic or epigenetic alterations, which ultimately lead to cancer.[37,38] However, the recent "cancer stem cell hypothesis" proposes the involvement of a minor population of cells with self-renewal capability in the pathogenesis of a variety of cancers, including HCC.[39] Moreover, it is considered that the development of tumors, at least in some cases of HCC, can be attributed to the propagation of the stem/progenitor cell component in hepatocarcinogenesis.[40] Given the close association between inflammation and carcinogenesis, it is reasonable that chronic and persistent tissue injury such as hepatitis viral infection might expand and activate the stem cell pool, thus predisposing the patient to the initiation of cancer.[41]

In the present study, using highly purified hepatic stem/progenitor cells and clonal analyses, we directly demonstrated that disrupted self-renewal drives transformation of hepatic stem/progenitor cells. We first confirmed that the 2 major self-renewal regulators of a broad range of stem cells, Bmi1 and the Wnt/β-catenin signaling pathway, also regulate the self-renewal of hepatic stem/progenitor cells in culture. Intriguingly, their effects were specific to hepatic stem/progenitor cells and did not enhance the colony-forming activity of the other cell fractions. These findings suggest that Bmi1 and ac-

Figure 9. Tumors derived from hepatic stem/progenitor cells. (*A*) Representative subcutaneous tumors (*left panel*, *arrows*) derived from 2 × 10^6 cells originating from H-CFU-Cs transduced with *Bmi1* in NOD/SCID mice. The tumors were dissected 12 weeks after the injection of 2 × 10^6 cells originating from H-CFU-Cs transduced with *Bmi1* (*right panel*; scale bar, 10 mm). (*B*) Representative livers transplanted with 2 × 10^6 cells originating from H-CFU-Cs transduced with either control (*lower*) or *Bmi1* (*upper*, scale bar, 10 mm). (*C*) H-CFU-Cs transduced with *Bmi1* or mutant *β-catenin* showed neoplastic transformation, which resulted in aggressive tumor growth. The tumor volume (*left panel*) and the survival curve of the recipient mice (*right panel*) are presented. (*D*) The subcutaneous tumor cells originating from H-CFU-Cs transduced with *Bmi1* or mutant *β-catenin* showed pleomorphic and hyperchromatic nuclei. Immunohistochemical analysis revealed that the tumors consisted of albumin$^+$ parenchymal cells (*red*) and CK7$^+$ glandular structures (*green*, scale bar, 100 μm). (*E*) Transplantation of EGFP$^+$ control cells contributed to the engraftment of albumin$^+$ hepatocytes (*upper panel*) and CK7$^+$ cholangiocytes (*lower panel*) (scale bar, 100 μm). (*F*) The histologic features of the liver tumors were similar to those of subcutaneous tumors. Proliferating albumin$^+$ cells (*red*) and CK7$^+$ (*green*) ductlike structures were intermingled. Clusters of cells expressing both albumin (*red*) and CK7 (*green*) simultaneously were also observed in tumors (scale bar, 100 μm).

tive β-catenin promote stem cell self-renewal but do not confer a growth advantage or self-renewal capacity on cells with limited growth and differentiation potential. Moreover, cell-cycle analysis revealed that the transduction of these 2 self-renewal regulators did not change the overall cell-cycle status of hepatic stem/progenitor cells, indicating that an accelerated cell-cycle progression, which usually plays a crucial role in the oncogenic process,[42] is not a principal cause in this case. Increased expression of the *Bmi1* gene and activation of the Wnt/β-catenin pathway are frequently observed in hepatoblastoma and HCC.[19,20] The functional specificity of Bmi1 and the Wnt/β-catenin in hepatic stem/progenitor cells again support the notion that stem cells are one of the major target cells of cancer development. Of note, tumors derived from H-CFU-Cs transduced with either *Bmi1* or mutant *β-catenin* exhibited similar histologic features. In addition, nests and clusters consisting of cells expressing both albumin and CK7, which might represent hepatic progenitor cells, were observed. Importantly, these histologic features were quite reminiscent of those of human cHCC-CC which is considered to be of stem/progenitor cell origin.[40]

Bmi1 has been well characterized as a self-renewal regulator of HSCs and NSCs.[30] Its role in the self-renewal of hepatic stem/progenitor cells was also evident in both gain-of-function and loss-of-function experiments in this study. Bmi1 is a potent negative regulator of the *Ink4a/Arf* locus, which encodes a cyclin-dependent kinase inhibitor, $p16^{Ink4a}$, and a tumor suppressor, $p19^{Arf}$, and regulates the cell cycle, apoptosis, and senescence.[43] In *Bmi1*-deficient mice, the expression of *Ink4a* and *Arf* is markedly increased, and deletion of the *Ink4a/Arf* locus substantially restores the self-renewal capacity of HSCs as well as NSCs.[44] Thus, Bmi1 regulates stem cell self-renewal by acting as a critical fail-safe mechanism against the $p16^{Ink4a}$- and $p19^{Arf}$-dependent premature loss of stem cells.[45,46] In the present study, overexpression of Bmi1 markedly repressed expression of $p16^{Ink4a}$ and $p19^{Arf}$ in hepatic stem/progenitor cells. Importantly, transcriptional disruption of the *Ink4a/Arf* locus is frequently observed in the process of hepatocaricinogenesis.[37,38] Loss of functional $p16^{Ink4a}$ and $p19^{Arf}$ might lead to excessive self-renewal of hepatic stem/progenitor cells, thereby driving the initiation of cancer as we observed in hepatic stem/progenitor cells overexpressing Bmi1.

Gain-of-function of Wnt/β-catenin signaling also resulted in successful expansion of hepatic stem/progenitor cells. This result appears to be consistent with a previous study showing that the nuclear translocation of β-catenin elicited by fibroblast growth factors induces a striking increase in the number of c-Kit^+ hepatic progenitors.[47] Mutant β-catenin efficiently accumulated in the nucleus. Although the expression of the Wnt/β-catenin targets, cyclin D1 and c-Myc, remained unchanged in H-CFU-C colonies expressing mutant β-catenin, a similar finding was reported in hyperplastic livers from mice expressing mutant *β-catenin* transgene.[48] Thus, the other targets might be relevant in the liver. In contrast, loss-of-function of Wnt/β-catenin signaling caused by the expression of Axin did not affect the self-renewal of hepatic stem/progenitor cells. It is possible that overexpression of Axin was not enough to repress Wnt/β-catenin signal below the level which led to impaired stem cell function. Another possibility would be that the Wnt/β-catenin signaling is dispensable in a physiologic setting. Further experiments are definitely necessary to determine the physiologic role of Wnt/β-catenin signaling. In either case, however, it is true that its activation strongly enhances the self-renewal capability and contributes to tumor initiation. In terms of the functional relation between the 2 self-renewal regulators, transduction of either one of them did not affect the expression or activity of the other. Thus, Bmi1 and Wnt/β-catenin pathway might independently regulate the self-renewal of hepatic stem/progenitor cells.

It has been reported that the special environment in culture might favor transformation.[49,50] This might be applied to our clonal H-CFU-C culture of 42 days. Although cultured H-CFU-Cs showed normal chromosomal numbers (data not shown), it would be necessary to determine whether additional events involuntarily occur and contribute to the initiation of cancer in collaboration with enhanced self-renewal signals. Involvement of facultative hepatic stem/progenitor cells such as oval cells in hepatocarcinogenesis has long been debated.[51,52] However, these studies, including the present study, took advantage of the transplantation assays of ex vivo–manipulated cells in evaluating carcinogenesis. To confirm whether the dysregulated self-renewal capability of hepatic stem/progenitor cells contributes to cancer initiation in vivo, it would be of great importance to trace the process of cancer initiation using mice with targeted expression of Bmi1 or mutant β-catenin in hepatic stem/progenitor cells.

In conclusion, our findings strongly support the cancer stem cell hypothesis that disruption of the self-renewal of hepatic stem/progenitor cells generates a cancer stem cell population as an early event, thereby contributing to the development of some HCCs. In this regard, regulators for self-renewal, Bmi1 and Wnt/β-catenin, might be potential targets for novel therapeutic approaches against cancer initiation and progression.

Supplementary data

Supplementary data associated with this article can be found, in the online version, at doi:10.1053/j.gastro.2007.06.016.

References

1. Shiojiri N, Lemire JM, Fausto N. Cell lineages and oval cell progenitors in rat liver development. Cancer Res 1991;51:2611–2620.
2. Zheng YW, Taniguchi H. Diversity of hepatic stem cells in the fetal and adult liver. Semin Liver Dis 2003;23:337–348.
3. Suzuki A, Zheng YW, Kaneko S, et al. Clonal identification and characterization of self-renewing pluripotent stem cells in the developing liver. J Cell Biol 2002;156:173–184.
4. Suzuki A, Zheng Y, Kondo R, et al. Flow-cytometric separation and enrichment of hepatic progenitor cells in the developing mouse liver. Hepatology 2000;32:1230–1239.
5. Weissman IL. Stem cells: units of development, units of regeneration, and units in evolution. Cell 2000;100:157–168.
6. Reya T, Morrison SJ, Clarke MF, Weissman IL. Stem cells, cancer, and cancer stem cells. Nature 2001;414:105–111.
7. Valk-Lingbeek ME, Bruggeman SW, van Lohuizen M. Stem cells and cancer; the polycomb connection. Cell 2004;118:409–418.
8. Iwama A, Oguro H, Negishi M, et al. Enhanced self-renewal of hematopoietic stem cells mediated by the polycomb gene product Bmi-1. Immunity 2004;21:843–851.
9. Park IK, Qian D, Kiel M, et al. Bmi-1 is required for maintenance of adult self-renewing haematopoietic stem cells. Nature 2003; 423:302–305.
10. Molofsky AV, Pardal R, Iwashita T, Park IK, Clarke MF, Morrison SJ. Bmi-1 dependence distinguishes neural stem cell self-renewal from progenitor proliferation. Nature 2003;425:962–967.
11. Leung C, Lingbeek M, Shakhova O, et al. Bmi1 is essential for cerebellar development and is overexpressed in human medulloblastomas. Nature 2004;428:337–341.
12. Pardal R, Clarke MF, Morrison SJ. Applying the principles of stem-cell biology to cancer. Nature Rev Cancer 2003;3:895–902.
13. Hussain SZ, Sneddon T, Tan X, Micsenyi A, Michalopoulos GK, Monga SP. Wnt impacts growth and differentiation in ex vivo liver development. Exp Cell Res 2004;292:157–169.
14. Tan X, Behari J, Cieply B, Michalopoulos GK, Monga SP. Conditional deletion of beta-catenin reveals its role in liver growth and regeneration. Gastroenterology 2006;131:1561–1572.
15. Monga SP, Pediaditakis P, Mule K, Stolz DB, Michalopoulos GK. Changes in WNT/beta-catenin pathway during regulated growth in rat liver regeneration. Hepatology 2001;33:1098–1109.
16. Zucman-Rossi J, Jeannot E, Nhieu JT, et al. Genotype-phenotype correlation in hepatocellular adenoma: new classification and relationship with HCC. Hepatology 2006;43:515–524.
17. Reya T, Clevers H. Wnt signaling in stem cells and cancer. Nature 2004;434:843–850.
18. Giles RH, van Es JH, Clevers H. Caught up in a Wnt storm: Wnt signaling in cancer. Biochim Biophys Acta 2001;1653:1–24.
19. Neo SY, Leow CK, Vega VB, et al. Identification of discriminators of hepatoma by gene expression profiling using a minimal dataset approach. Hepatology 39:944–953.
20. Taniguchi K, Roberts LR, Aderca IN, et al. Mutational spectrum of beta-catenin, AXIN1, and AXIN2 in hepatocellular carcinomas and hepatoblastomas. Oncogene 2002;21:4863–4871.
21. Dean M, Fojo T, Bates S. Tumour stem cells and drug resistance. Nature Rev Cancer 2005;5:275–284.
22. Xin L, Lawson DA, Witte ON. The Sca-1 cell surface marker enriches for a prostate-regenerating cell subpopulation that can initiate prostate tumorigenesis. Proc Natl Acad Sci U S A 2005; 102:6942–6947.
23. Shackleton M, Vaillant F, Simpson KJ, et al. Generation of a functional mammary gland from a single stem cell. Nature 2006; 439:84–88.
24. Zender L, Spector MS, Xue W, et al. Identification and validation of oncogenes in liver cancer using an integrative oncogenomic approach. Cell 2006;125:1253–1267.
25. Lee JS, Heo J, Libbrecht L, et al. A novel prognostic subtype of human hepatocellular carcinoma derived from hepatic progenitor cells. Nat Med 2006;12:410–416.
26. Harada N, Tamai Y, Ishikawa T, et al. Intestinal polyposis in mice with a dominant stable mutation of the beta-catenin gene. EMBO J 1999;18:5931–5942.
27. Katayama K, Wada K, Miyoshi H, et al. RNA interfering approach for clarifying the PPARgamma pathway using lentiviral vector expressing short hairpin RNA. FEBS Lett 2004;560:178–182.
28. Chinzei R, Tanaka Y, Shimizu-Saito K, et al. Embryoid-body cells derived from a mouse embryonic stem cell line show differentiation into functional hepatocytes. Hepatology 2002;36:22–29.
29. Kakinuma S, Tanaka Y, Chinzei R, et al. Human umbilical cord blood as a source of transplantable hepatic progenitor cells. Stem Cells 2003;21:217–227.
30. Park IK, Morrison SJ, Clarke MF. Bmi1, stem cells, and senescence regulation. J Clin Invest 2004;113:175–179.
31. Shtutman M, Zhurinsky J, Simcha I, et al. The cyclin D1 gene is a target of the beta-catenin/LEF-1 pathway. Proc Natl Acad Sci U S A 1999;96:5522–5527.
32. He TC, Sparks AB, Rago C, et al. Identification of c-MYC as a target of the APC pathway. Science 1998;281:1509–1512.
33. Monga SP, Monga HK, Tan X, Mule K, Pediaditakis P, Michalopoulos GK. Beta-catenin antisense studies in embryonic liver cultures: role in proliferation, apoptosis, and lineage specification. Gastroenterology 2003;124:202–216.
34. Wicha MS, Liu S, Dontu G. Cancer stem cells: an old idea—a paradigm shift. Cancer Res 2006;66:1883–1890.
35. Jamieson CH, Weissman IL, Passegue E. Chronic versus acute myelogenous leukemia: a question of self-renewal. Cancer Cell 2004;6:531–533.
36. Kato Y, Iwama A, Tadokoro Y, et al. Selective activation of STAT5 unveils its role in stem cell self-renewal in normal and leukemic hematopoiesis. J Exp Med 2005;202:169–179.
37. Bruix J, Boix L, Sala M, Llovet JM. Focus on hepatocellular carcinoma. Cancer Cell 2004;5:215–219.
38. Roberts LR, Gores GJ. Hepatocellular carcinoma: molecular pathways and new therapeutic targets. Semin Liver Dis 2005;25: 212–225.
39. Al-Hajj M, Clarke MF. Self-renewal and solid tumor stem cells. Oncogene 2004;23:7274–7282.
40. Theise ND, Yao JL, Harada K, et al. Hepatic 'stem cell' malignancies in adults: four cases. Histopathology 2003;43:263–271.
41. Beachy PA, Karhadkar SS, Berman DM. Tissue repair and stem cell renewal in carcinogenesis. Nature 2004;432:324–331.
42. Sherr CJ. Cancer cell cycles. Science 1996;274:1672–1677.
43. Jacobs JJ, Kieboom K, Marino S, DePinho RA, van Lohuizen M. The oncogene and Polycomb-group gene bmi-1 regulates cell proliferation and senescence through the ink4a locus. Nature 1999;397:164–168.
44. Oguro H, Iwama A, Morita Y, Kamijo T, van Lohuizen M, Nakauchi H. Differential impact of Ink4a and Arf on hematopoietic stem cells and their bone marrow microenvironment in Bmi1-deficient mice. J Exp Med 2006;203:2247–2253.
45. Valk-Lingbeek ME, Bruggeman SW, van Lohuizen M. Stem cells and cancer; the polycomb connection. Cell 2004;118:409–418.
46. Molofsky AV, He S, Bydon M, Morrison SJ, Pardal R. Bmi-1 promotes neural stem cell self-renewal and neural development but not mouse growth and survival by repressing the p16Ink4a and p19Arf senescence pathways. Genes Dev 2005;19:1432–1437.
47. Sekhon SS, Tan X, Micsenyi A, Bowen WC, Monga SP. Fibroblast growth factor enriches the embryonic liver cultures for hepatic progenitors. Am J Pathol 2004;164:2229–2240.
48. Cadoret A, Ovejero C, Saadi-Kheddouci S, et al. Hepatomegaly in transgenic mice expressing an oncogenic form of beta-catenin. Cancer Res 2001;61:3245–3249.

49. Bellusci S, Moens G, Gaudino G, et al. Creation of an hepatocyte growth factor/scatter factor autocrine loop in carcinoma cells induces invasive properties associated with increased tumorigenicity. Oncogene 1994;9:1091–1099.
50. Huang C, Ma WY, Dong Z. Requirement for phosphatidylinositol 3-kinase in epidermal growth factor-induced AP-1 transactivation and transformation in JB6 P+ cells. Mol Cell Biol 1996;16: 6427–6435.
51. Goyette M, Faris R, Braun L, Hixson D, Fausto N. Expression of hepatocyte and oval cell antigens in hepatocellular carcinomas produced by oncogene-transfected liver epithelial cells. Cancer Res 1990;50;4809–4817.
52. Dumble ML, Croager EJ, Yeoh GC, Quail EA. Generation and characterization of p53 null transformed hepatic progenitor cells: oval cells give rise to hepatocellular carcinoma. Carcinogenesis 2002;23:435–445.

Received November 15, 2006. Accepted May 31, 2007.

Address requests for reprints to: Hideki Taniguchi, MD, PhD, Department of Regenerative Medicine, Graduate School of Medicine, Yokohama City University, 3-9 Fukuura, Kanazawa-ku, Yokohama 236-0004, Japan. e-mail: rtanigu@med.yokohama-cu.ac.jp; fax: (81) 45-787-8963.

All authors declare that they have no conflict of interest to disclose.

Supported in part by the National Leading Project for Realization of "Regenerative Medicine"; Grants-in-Aid for Scientific Research from the Ministry of Education, Culture, Sports, Science, and Technology, Japan (14207046, 14081201, 16659340); Core Research for Evolutional Science and Technology (CREST) of Japan Science and Technology Corporation (JST); and grants from Mitsubishi Foundation and Sankyo Foundation of Life Science.

The authors thank Yohei Morita, Yuji Yamazaki, Makoto Otsu, Akihide Kamiya, Sei Kakinuma, and Rei Hirochika for technical assistance.

Available online at www.sciencedirect.com
ScienceDirect
Biochemical and Biophysical Research Communications xxx (2007) xxx–xxx
BBRC
www.elsevier.com/locate/ybbrc

VEGF promotes tumorigenesis and angiogenesis of human glioblastoma stem cells

Naoki Oka [a], Akio Soeda [a,*], Akihito Inagaki [b], Masafumi Onodera [c], Hidekazu Maruyama [c], Akira Hara [d], Takahiro Kunisada [b], Hideki Mori [d], Toru Iwama [a]

[a] *Department of Neurosurgery, Gifu University School of Medicine, 1-1 Yanagido, Gifu City, Gifu 501-1194, Japan*
[b] *Department of Tissue and Organ Development Regeneration and Advanced Medical Science, Gifu University School of Medicine, Gifu City, Gifu 501-1194, Japan*
[c] *Department of Hematology, Institutes of Clinical Medicine, University of Tsukuba, Tsukuba City, Ibaragi 305-8577, Japan*
[d] *Department of Tumor Pathology, Gifu University School of Medicine, Gifu City, Gifu 501-1194, Japan*

Received 2 June 2007

Abstract

There is increasing evidence for the presence of cancer stem cells (CSCs) in malignant brain tumors, and these CSCs may play a pivotal role in tumor initiation, growth, and recurrence. Vascular endothelial growth factor (VEGF) promotes the proliferation of vascular endothelial cells (VECs) and the neurogenesis of neural stem cells. Using CSCs derived from human glioblastomas and a retrovirus expressing VEGF, we examined the effects of VEGF on the properties of CSCs *in vitro* and *in vivo*. Although VEGF did not affect the property of CSCs *in vitro*, the injection of mouse brains with VEGF-expressing CSCs led to the massive expansion of vascular-rich GBM, tumor-associated hemorrhage, and high morbidity, suggesting that VEGF promoted tumorigenesis via angiogenesis. These results revealed that VEGF induced the proliferation of VEC in the vascular-rich tumor environment, the so-called stem cell niche.

Keywords: Glioblastoma; Cancer stem cell; Angiogenesis; Vascular endothelial growth factor; Microenvironment; Gene delivery systems; Stem cell niche

Malignant gliomas, especially glioblastomas multiforme (GBM), are highly aggressive. They are the most lethal primary brain tumors with a median survival of less than 12 months [1]. Human gliomas contain a subpopulation of cells with stem cell-like properties, designated cancer stem cells (CSCs), that may play an important role in tumorigenesis and tumor recurrence [2–6]. Because vascular endothelial growth factors (VEGF) and their receptors (VEGFR) are important paracrine factors involved in tumorigenesis and angiogenesis, they may be possible targets for therapeutic intervention [7–9]. However, it remains unknown whether VEGF affect the proliferation and differentiation of CSCs and tumors derived from these cells.

We isolated and characterized multipotent, self-renewing cells derived from fresh human GBM. Established X01GB cells formed proliferating tumor spheres, could be serially passaged in proliferation medium containing epidermal growth factor (EGF) and basic fibroblast growth factor (FGF-2), and differentiated into both neurons and astrocytes in differentiation medium containing fetal bovine serum (FBS). After orthotopic implantation into the brains of immunodeficient mice, the CSCs grew into tumors that were a phenocopy of the original GBM. To investigate the role of VEGF in human CSCs, we used a VEGF-expressing retrovirus in *in vitro* and *in vivo* models of gliomagenesis. We show that while retroviral VEGF did not affect the property of stem cells *in vitro*, the transplantation of VEGF-expressing X01GB cells into mouse brains induced the massive expansion of vascular-rich GBM, tumor-associated hemorrhage, and high morbidity.

* Corresponding author.
E-mail address: ccd29400@nyc.odn.ne.jp (A. Soeda).

0006-291X/$ - see front matter © 2007 Elsevier Inc. All rights reserved.
doi:10.1016/j.bbrc.2007.06.094

Materials and methods

Preparation of recombinant retroviruses. Human VEGF165 cDNA [10] was kindly provided by Dr. M. Shibuya (Institute of Medical Science, University of Tokyo, Japan). The retroviral vector GCDNsamIRES/EGFP, which includes a long terminal repeat and a primer binding site derived from the mouse endogenous retroviruses PCMV and dl587rev, respectively, was constructed to express enhanced green fluorescent protein (EGFP) as a marker [11]. To construct the vector expressing human VEGF, a BamHI fragment containing a full-length VEGF cDNA was inserted into a corresponding site in the vector; this was designated pDNhVEGF. Methods for producing recombinant retroviruses packaged into vesicular stomatitis virus G (VSV-G) protein are described elsewhere [12]. This vector was converted to the corresponding retrovirus by transduction into 293gpg cells [12,13], yielding a viral titer of 1.95×10^6 infectious units/ml as assessed in Jurkat cells.

Establishment and transduction of CSCs. Prior informed consent was obtained from the GBM sample donor and the study was approved by the Medical Review Board of Gifu University. Within 2 h of tumor removal, tissues were minced with scissors, incubated in 0.05% trypsin (GIBCO-Invitrogen, La Jolla, CA) in 0.1 mM EDTA (20 min, 37 °C), and washed. Cells were then dissociated in phosphate-buffered saline (PBS) to eliminate cell debris and triturated in the same solution in a fire-polished Pasteur pipette. Cells passed through a 100-μm strainer (Falcon, Oxnard, CA) were seeded (1×10^5/ml) into Falcon culture flasks and grown in medium containing DMEM/F12 (GIBCO/Invitrogen, NY, USA), penicillin G, streptomycin sulfate, B-27 (1:50; GIBCO/Invitrogen), recombinant human fibroblast growth factor (hFGF-2, 20 ng/ml; R&D Systems, Minneapolis, MN, USA), recombinant human epidermal growth factor (hEGF, 20 ng/ml; R&D Systems), and leukemia inhibitory factor (LIF, 1000 U/ml). The medium was replaced every 3 days with identical fresh medium. Spheres were counted under a phase-contrast microscope (Olympus IMT-2, Tokyo, Japan). Passage was by trituration in a fire-polished Pasteur pipette; the cells were reseeded into fresh proliferation medium and maintained in a 37 °C incubator with 95% air and 5% CO_2.

After 50 passages of the tumor spheres, for transduction with DNEGFP-VEGF, 1×10^6 cells were plated in 10 ml culture medium and 50 μl DNEGFP-VEGF supernatant (multiplicity of infection (MOI) = 1). Two days post-transduction, the cells were analyzed by FACS Vantage (BD Bioscience, CA, USA). For the immunostaining of tumor spheres, 1–10 spheres were transferred to poly-L-lysine (Sigma)-coated 24-well dishes (Falcon, Oxnard, CA) in medium containing 10% FBS to facilitate anchorage. After 4 h, attached spheres were fixed in 4% paraformaldehyde in PBS (15 min), washed in PBS, and incubated for 1 h in blocking solution (2% skim milk, 1% normal goat serum, 0.2% bovine serum albumin (BSA), and 0.2% Triton X-100 in PBS). For triple-label immunostaining, primary antibodies were diluted in PBS containing 2% skim milk and 0.2% Triton X-100. Cells in 24-well dishes were incubated for 24 h at 4 °C, secondary antibodies were added, and the dishes were incubated for 2 more hours at 37 °C. The neurospheres were immunostained with human anti-nestin (rabbit polyclonal antibody (pAb), 1:200; Chemicon, Temecula, CA) for neural stem and progenitor cells, with anti-βIII-tubulin (mouse mAb, 1:200; Chemicon) for neurons, or with anti-glial fibrillary acidic protein (GFAP; rabbit pAb, 1:500; DAKO, Glostrup, Denmark) for astrocytes; and then with Alexa fluorophore-conjugated secondary antibodies (1:1000; Molecular Probes, Eugene, OR). For the differentiation of tumor spheres, cells were fed with FBS-supplemented medium every 2 days. After 7 days, immunocytochemistry was performed as described above. Cells were additionally immunostained with Hoechst 33342 to identify all nuclei and permit their counting in at least five microscopic fields per specimen. Cellular self-renewal ability was evaluated with a modified limiting dilution assay described previously [3].

Transplantation into immunodeficient mice and survival study. Our experimental procedures involving animals followed the guidelines of the Animal Experimental Committee of Gifu University. Tumorigenicity was determined by injecting brain tumor-derived CSCs (X01GB) orthotopically into non-obese diabetic-severe combined immunodeficiency (NOD-SCID) mice (SLC, Shizuoka, Japan). EGFP-VEGF-X01GB or EGFP-X01GB cells were injected into the brain of katamine-anesthetized NOD-SCID mice; 2 μl of a cell suspension (1×10^8 cells/ml) in proliferation medium were delivered into the right striatum (1 μl/min) using a stereotactic instrument (SR-60, Narishige, Tokyo, Japan) and a Hamilton syringe. The injection coordinates were 3 mm to the right of the midline and 3 mm anterior to the lamda, at a depth of 3 mm. Mice injected with EGFP-X01GB ($n = 6$) or EGFP-VEGF-X01GB ($n = 8$) were monitored daily for signs of morbidity, e.g. weight loss, seizures, posturing, and nasal and/or periorbital hemorrhage and killed at the first sign of morbidity. Their brains were examined histologically for the presence of tumor. Kaplan–Meier survival curves were designed, and the survival of EGFP-VEGF-X01GB and EGFP-X01GB xenografted mice was compared statistically using the log-rank test and GraphPad Prism 4 software (GraphPad Software, CA, USA).

Immunohistochemical analysis of brain tissues. Tumor samples were fixed in 4% paraformaldehyde, paraffin-embedded, and cut into 3-μm sections. For hematoxylin–eosin staining, they were first stained with Mayer's hematoxylin (1 min) and then counterstained with alcoholic eosin. For immunohistochemical studies, deparaffinized sections were washed in Tris-buffered saline (TBS), endogenous peroxidase was neutralized with 3% H_2O_2 in methanol (15 min) after 15-min antigen retrieval in citrate buffer in a microwave at 500 W. Sections were blocked with 1% bovine serum albumin in TBS and then treated overnight at 4 °C with the following primary antibodies; anti-human nestin (mouse monoclonal antibody (mAb), 5 μg/ml; R&D Systems) for neural stem cells, anti-human Ki-67 (mouse mAb, 1:50; DAKO) for proliferative indices, anti-GFAP (mouse mAb, 1:500; DAKO) for astrocytes, and anti-human βIII-tubulin (mouse mAb, 1:500; Chemicon) for neurons. After treatment with biotinylated secondary antibody and HRP-linked streptavidin (LSAB2 kit, DAKO), color reactions were performed with peroxidase-substrate 3,3′-diaminobenzidine (DAB, DAKO). For vascular studies, tumor samples were snap-frozen, cut into 5-μm frozen sections, fixed, and immunostained with anti-mouse CD31 (rabbit polyclonal antibody, 1:100; Santa Cruz, CA, USA) and anti-human CD31 (mouse mAb, 1:30; DAKO). For periodic acid-Schiff (PAS) staining, the sections were deparaffinized, washed in TBS, stained with 0.5% periodic acid (5 min), stained (15 min) with Schiff's reagent (Muto Chemical, Tokyo, Japan), and washed three times (3 min each) in sulfurous acid solution. All sections were counter-stained with Mayer's hematoxylin.

Reverse transcription polymerase chain reaction (RT-PCR). Total RNA was purified from cultures at various times using Isogen (Nippon Gene, Tokyo, Japan) for cDNA synthesis and the manufacturer's instructions. cDNA was prepared from RNA templates (5 μg) after reverse transcription, using oligo (dT) primers and Super Script II reverse transcriptase (Invitrogen, NY, USA). The product (100 ng) was subjected to PCR with rTaq polymerase (Takara Bio, Shiga, Japan) and each PCR product (10 μl) was electrophoresed on 1% agarose gels and stained with ethidium bromide.

Forward and reverse primer sequences for specific amplifications are shown in Table 1. The amplification conditions for VEGF-A were initial denaturation at 94 °C for 2 min, 35 cycles of denaturation at 94 °C for 30 s, annealing at 60 °C for 30 s, and extension at 72 °C for 60 s [8]; for VEGF-B they were initial denaturation at 95 °C for 1 min, 30 cycles of denaturation at 95 °C for 60 s, annealing at 60 °C for 60 s, and extension at 72 °C for 90 s [14]; for VEGFR1 (Flt-1) and VEGFR2 (Flk-1) they were initial denaturation at 94 °C for 2 min, 35 cycles of denaturation at 94 °C for 90 s, annealing at 60 °C for 3 min, and extension at 72 °C for 4 min [15]; for β-actin they were initial denaturation at 94 °C for 2 min, 30 cycles of denaturation at 94 °C for 30 s, annealing at 60 °C for 30 s, and extension at 72 °C for 60 s.

Table 1
Forward and reverse primer sequences for specific amplifications

mRNA targets	Oligonucleotides	Product size (bp)
VEGF-A	Forward: 5′-ATCACGAAGTGGTGAAGTTC-3′ Reverse: 5′-TGCTGTAGGAAGCTCATCTC-3′	265
VEGF-B	Forward: 5′-CCATGAGCCCTCTGCTCCGCC-3′ Reverse: 5′-GCCATGTGTCACCTTCGCAGC-3′	678
VEGFR1	Forward: 5′-GAAGGCATGAGGATGAGAGC-3′ Reverse: 5′-CAGGCTC ATGAACTTG AAAGC-3′	324
VEGFR2	Forward: 5′-GTCAAGGGAAAGACTAC GTTGG-3′ Reverse: 5′-AGCAGTCCAGCATGGTCTG-3′	591
β-Actin	Forward: 5′-GAAAGTAGGGACCTCAGAGG-3′ Reverse: 5′-CTGTCCTCCCTCACACGTCA-3′	218

Results

VEGF has no effect on the properties of CSCs in vitro

X01GB-CSCs from a GBM patient were serially cultured in proliferation medium containing growth factor; they were able to self-renew and to differentiate into cells with multilineage properties (data not shown). The sphere cells were immunoreactive with neural stem cells (NSCs) and the CSC marker nestin (Fig. 1A and B). In differentiation medium containing FBS, spheres differentiated not only into neurons and glia but also into cells expressing both neuronal and glial cell markers (Fig. 1C). Upon orthotopic transplantation into immunodeficient mice, the X01GB cells initiated new tumors that were a phenocopy of the original GBM and exhibited extensive infiltrative capacity (Fig. 1D). Based on these findings, our X01GB cells fulfilled the criteria for CSCs [2–6].

To determine whether VEGF has an effect on the properties of stem cells within CSC populations *in vitro*, we first investigated their self-renewal capacity in the presence (20 ng/ml) and absence of VEGF. Dissociated X01GB cells formed floating tumor spheres in a VEGF-independent manner and there was no significant difference in their number (data not shown). To further elucidate the effect of VEGF, we transfected the EGFP-VEGF gene into X01GB CSCs (EGFP-VEGF-X01GB) using a retrovirus vector. RT-PCR analysis showed that VEGF-A was highly expressed in EGFP-VEGF-X01GB cells; there was no significant difference with respect to the expressions of VEGF-B, VEGFR1 (Flt-1), and VEGFR2 (Flk-1) (Fig. 2A). Upon flow cytometric analysis, more than 40% of the transfected cells expressed EGFP after one round of transduction; after 6-month culture, more than 90% continued to express EGFP (Fig. 2B). These enriched tumor spheres expressed

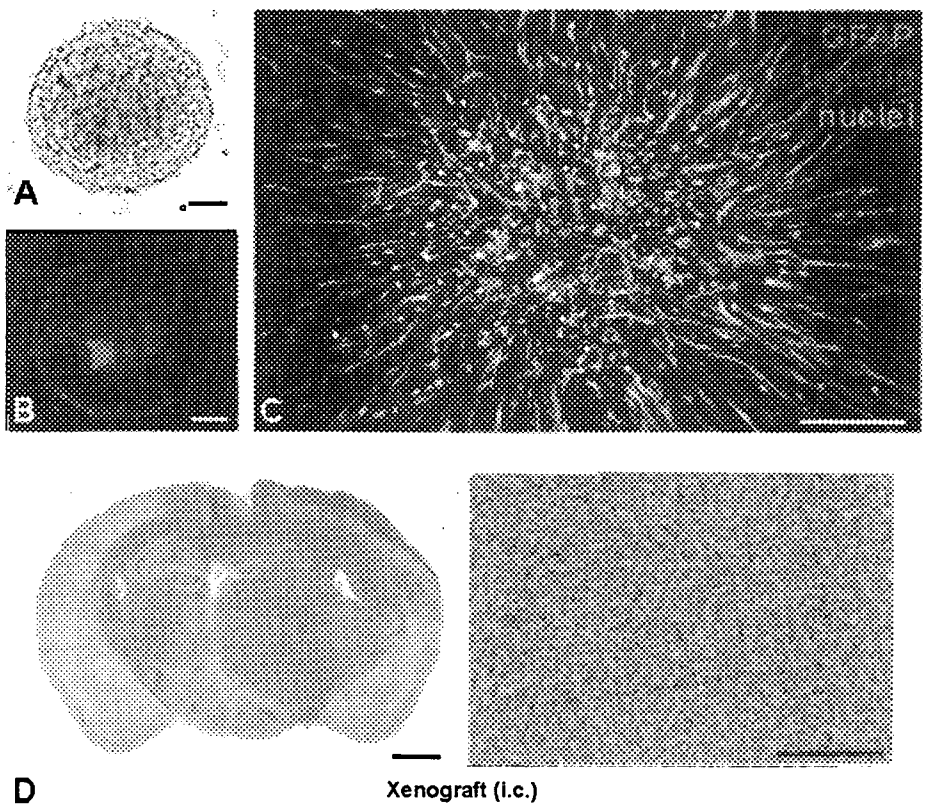

Fig. 1. The sphere shown is from line X01GB (A). There is positive immunostaining for the neural progenitor marker nestin, indicating the presence of undifferentiated stem cells in the spheres (B). The cells gave rise not only to neurons and glia but also to cells expressing both neuronal and glial cell markers (C). Transplanted spheres from X01GB developed and recapitulated the histopathological properties of the parental GBM (D). In (C), GFAP staining is seen as green, staining for βIII-tubulin as red, and nuclei are stained blue. Scale bars: 1 mm (D, left), 100 μm (D, right), 50 μm (A–C).

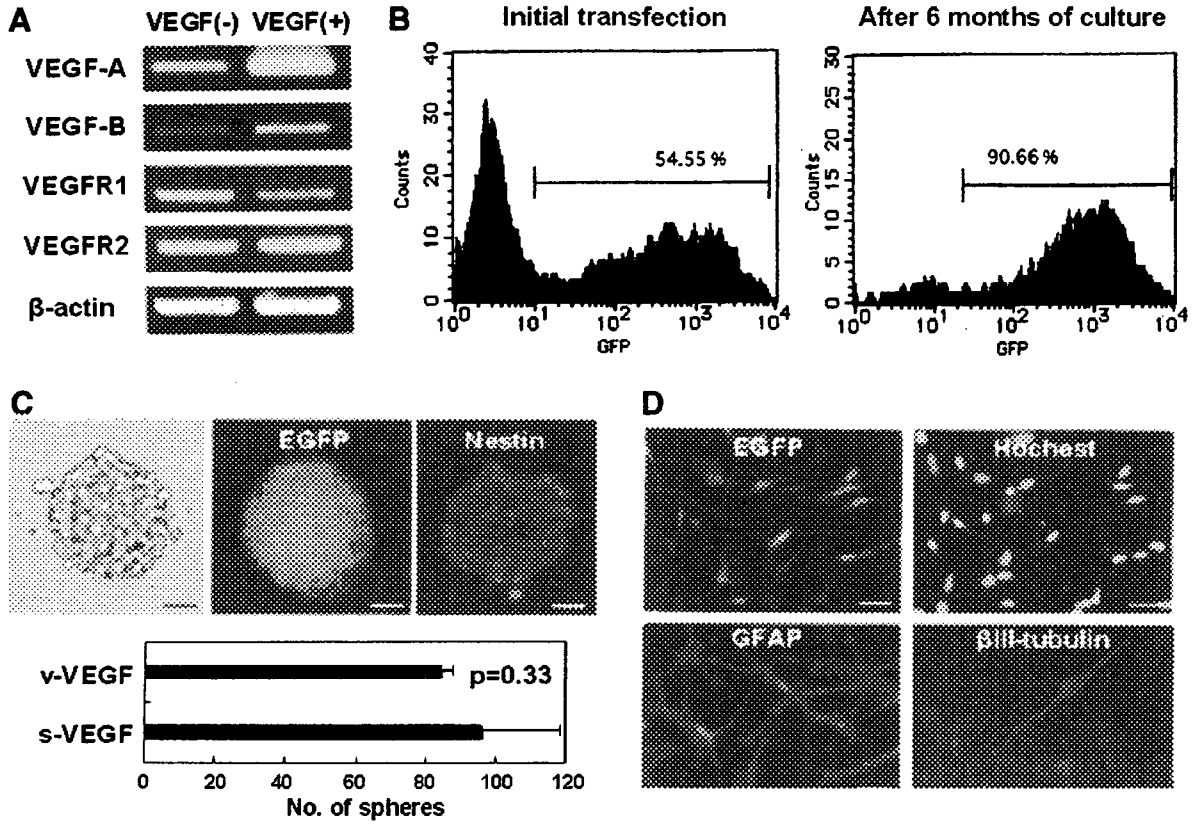

Fig. 2. (A) RT-PCR showed that EGFP-VEGF-X01GB (VEGF(+)) cells expressed VEGF-A with high efficiency; there was no difference between VEGF(+) and VEGF(−) cells with respect to the expression of VEGF-B, VEGFR-1 (Flt-1), and VEGFR-2 (Flk-1) genes. (B) Efficiency of EGFP-VEGF reporter gene expression in X01GB CSCs. About 55% of infected cells expressed EGFP (left); enriched cells also expressed EGFP even after prolonged culture (right). (C) A sphere from line EGFP-VEGF-X01GB. EGFP-expressing spheres are positive for the neural progenitor marker nestin. There was no significant difference between cells treated with soluble VEGF (s-VEGF) and cells expressing viral VEGF (v-VEGF) with respect to their self-renewal ability ($p = 0.33$). (D) Under differentiated culture conditions in the presence of serum, a significant portion of the differentiated cells continued to express EGFP (nuclei are Hoechst-stained). These cells were also positive for glial (GFAP) and/or neuronal markers (βIII-tubulin). Scale bars: 50 μm (C), 25 μm (D).

both EGFP and nestin, and like the X01GB tumor spheres, they could be serially passaged (Fig. 2C). There was no significant difference in the self-renewal capacity of soluble VEGF-X01GB- and EGFP-VEGF-X01GB cells (Fig. 2C). Under differentiation conditions, like untransfected X01GB cells, they differentiated and expressed glial and neuronal markers (Fig. 2D). These results suggested that this retroviral transduction method allowed CSCs to express EGFP/VEGF efficiently without interfering with their sphere formation- and differentiation abilities *in vitro*.

VEGF induces vascular-rich GBM tumors in mice with associated hemorrhage and high morbidity

We next investigated whether VEGF affected tumorigenesis, angiogenesis and morbidity *in vivo*. Cells were stereotactically injected into the brains of immunodeficient mice. Kaplan–Meier survival curves revealed that at less than 64-days post-injection, all mice transplanted with EGFP-VEGF-X01GB cells showed signs of tumor-induced morbidity; mice injected with EGFP-X01GB cells did not (Fig. 3A). Most of the brains injected with VEGF-expressing cells displayed gross evidence of tumor-associated hemorrhage (Fig. 3B and C). These results suggested that VEGF promoted tumor-associated hemorrhage and induced high morbidity.

We next performed a histopathologic investigation of the characteristics of tumors derived from EGFP-VEGF-X01GB cells. The tumors exhibited marked vascular proliferation and pseudopalisading necrosis; the density and complexity of new blood vessels adjacent to and within the tumors was evidence for high angiogenesis (Fig. 4A and B). To investigate the structure and features of these tumor vessels we used PAS staining, which has strong affinity for polysaccharides in the basement membrane. In EGFP-VEGF-X01GB- but not EGFP-X01GB-transplanted mice, the tumor vessels were hyper-angiogenic and there was a reticular meshwork surrounding the tumor cells (Fig. 4C and D), suggesting that tumor angiogenesis was due to the formation of VEC-lined vessels. To determine whether these VECs derived from the transplanted human CSCs or from the mice *per se*, we used the mouse-specific (no cross-reactivity with human) and human-specific (no cross-reactivity with murine) anti-vascular endothelial marker CD31. We found that in EGFP-VEGF-X01GB xenografted mice, VECs in the tumor ves-

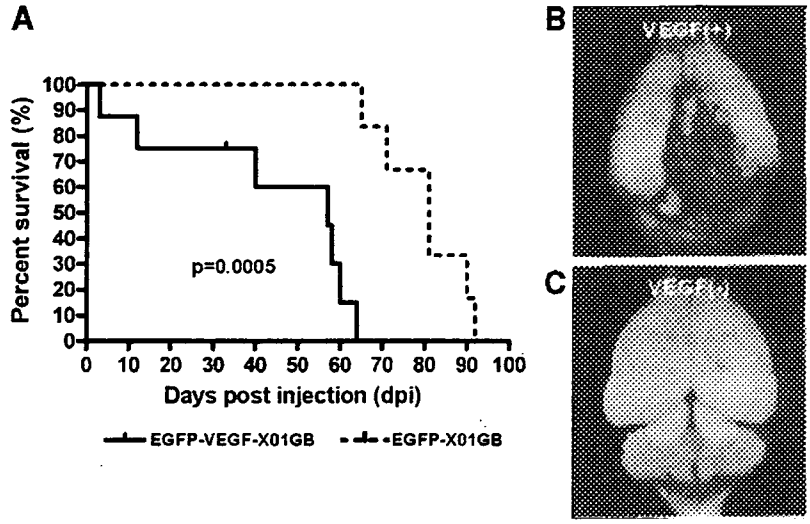

Fig. 3. Kaplan–Meier survival curve showing the rapid onset of high tumor-induced morbidity (A). All mice injected with EGFP-VEGF-X01GB cells showed signs of tumor-induced morbidity within 64-days post-injection; mice injected with EGFP-X01GB did not. The mean survival after EGFP-VEGF-X01GB injection was 57 days; mice injected with EGFP-X01GB survived for a mean of 81 days. The p value (log-rank test) was 0.0005, the hazard ratio was 4.470 (the 95% CI was 3.505–84.81). Tumor-associated hemorrhage involving the brain surface was seen in mice transplanted with EGFP-VEGF-X01GB cells (5/8, B), but not in mice injected with EGFP-X01GB cells (0/6, C).

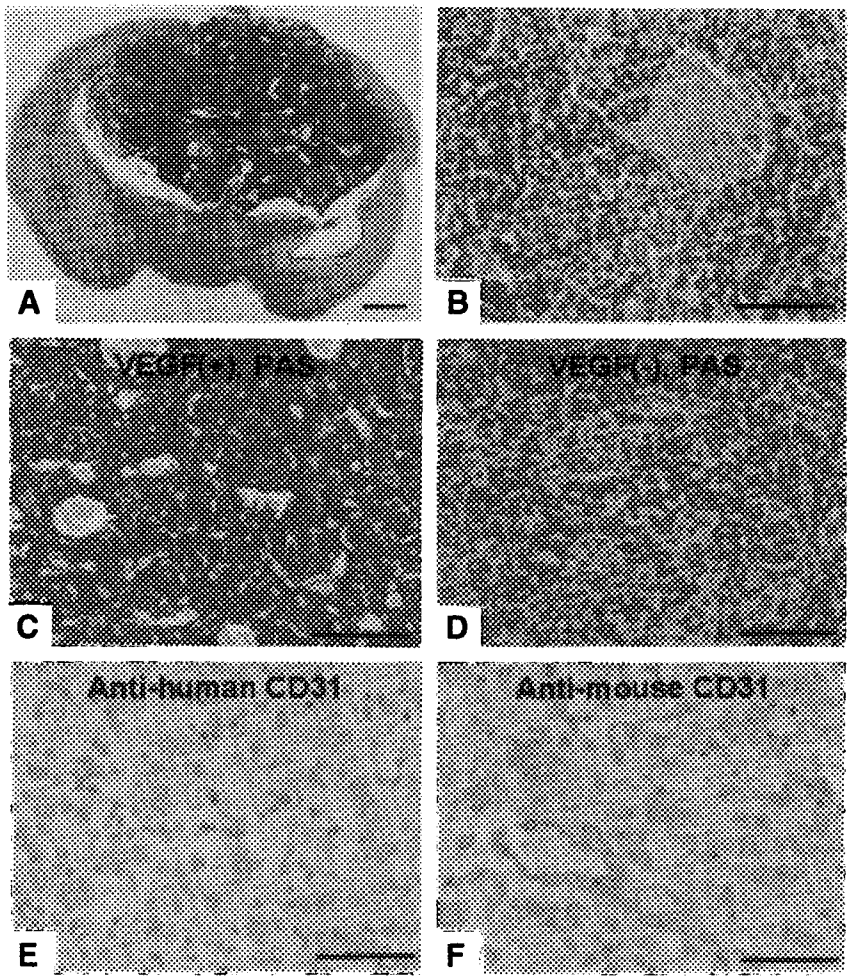

Fig. 4. (A) Gross view of a mouse brain 8 weeks after injection. The transplanted tumors were vascular-rich compared to the tumors in mice subjected to non-infected xenografts (B, see Fig. 1D). PAS staining showed hyper-angiogenesis and dense reticular networks, reminiscent of sinusoid, supplying blood to the tumors (C). In contrast, there was less angiogenesis in tumors developed from EGFP-X01GB xenografts (D). Immunohistochemically, VECs in the tumor vessels were negative for human-specific anti CD31 (E) and positive for mouse-specific anti CD31 (F). Scale bars: 1 mm (A), 100 μm (B–D), 50 μm (E,F).

sels were negative for human- and positive for mouse CD31, indicating that they derived from the murine brain (Fig. 4E and F).

Discussion

Here we showed that VEGF treatment of stem cells derived from human GBM promoted vascular formation, tumor-associated hemorrhage, and tumorigenesis. The VEGF signaling pathway plays an important role in gliomagenesis and activation is closely related with brain tumor development via vascular formation [16,17], observations that coincide with our findings that VEGF promoted tumor angiogenesis resulting in the rapid growth of GBMs.

Similarities between stem cells and cancer cells with respect to their self-renewal capacity and multi-potential cell fate gave rise to the concept of CSCs [18,19]. NSCs and CSCs may be under a high degree of regulation by their extracellular microenvironments; this may promote their self-renewal and retention in the undifferentiated state [20–22] suggested that VECs are important in tissue architecture, that they specify the fate of different neighboring cell types including NSCs, and that the microenvironment, termed stem cell niche, regulates NSC proliferation and neurogenesis, possibly through the secretion of neurotrophic factor(s). NSCs are not randomly distributed throughout the brain, rather, they are concentrated around blood vessels [20]. Furthermore, most cancers including GBMs are well vascularized and their malignancy depends on vascular formation [17]. However, the role of VECs with respect to CSCs remains to be elucidated.

We found that VEGF promoted tumor angiogenesis by acting on murine VECs, forming a central lumen, and elaborating a new basement membrane. This results in the development of new blood vessels and bleeding [16]. VEGF is a highly specific endothelial cell mitogen that has been shown to promote VEC proliferation, migration, and survival, resulting in tumor angiogenesis, a requirement for glioma growth [23]. In glioma patients, effective therapeutic intervention requires the development of treatments that target and eliminate CSCs, and the VEGF gene and other angiogenic factors may represent valuable molecular targets [8,9]. Further, elucidating the VEC-secreted signaling molecules that elicit CSC proliferation may be a step forward in CSC biology, in particular for understanding their niches and their optimal use in anti-angiogenic treatments [24].

In this study, we used the simplified retroviral vector GCDNsap that was engineered to be resistant to de novo methylation. It was packaged into vesicular stomatitis virus G protein (VSV-G) to transfect the EGFP/VEGF gene into CSCs. This system allowed for the genetic modification of NSCs; the transduction rate was high in the absence of FBS during the transduction process [12]. Using these genetic modifications, the resultant EGFP/VEGF-expressing X01GB cells, like untransfected X01GB cells, had the ability for self-renewal and *in vitro* differentiation. As the retrovirus expressed high levels of fluorescent EGFP reporter genes, we were able to identify infected cells and their progeny (data not shown). Our findings suggest that this gene transfer system is a useful tool for the genetic modification of CSCs.

Targeting the pathways that regulate aberrant self-renewal represents an alternative approach to attacking CSCs. Success will depend on the ability to develop drugs that selectively target CSCs and/or their niche [25]. Insight into the relationship between CSCs and their niches, important for an understanding of the formation and growth of human brain tumors, may also help to identify novel tumor cell markers useful for their diagnosis and treatment. Effective treatment may require the targeting and elimination of CSCs in a patient-specific manner.

Acknowledgments

We thank Tsutomu Motohashi, Hitomi Aoki, Ayako Suga, and Kyoko Takahashi for their technical assistance and Ms. Ursula A. Petralia for editing the manuscript.

References

[1] M. Lacroix, D. Abi-Said, D.R. Fourney, Z.L. Gokaslan, W. Shi, F. DeMonte, F.F. Lang, I.E. McCutcheon, S.J. Hassenbusch, E. Holland, K. Hess, C. Michael, D. Miller, R. Sawaya, A multivariate analysis of 416 patients with glioblastoma multiforme: Prognosis, extent of resection, and survival, J. Neurosurg. 95 (2001) 190–198.

[2] H.D. Hemmati, I. Nakano, J.A. Lazareff, M. Masterman-Smith, D.H. Geschwind, M. Bronner-Fraser, H.I. Kornblum, Cancerous stem cells can arise from pediatric brain tumors, Proc. Natl. Acad. Sci. USA 100 (2003) 15178–15183.

[3] S.K. Singh, I.D. Clarke, M. Terasaki, V.E. Bonn, C. Hawkins, J. Squire, P.B. Dirks, Identification of a cancer stem cell in human brain tumors, Cancer Res. 63 (2003) 5821–5828.

[4] S.K. Singh, C. Hawkins, I.D. Clarke, J.A. Squire, J. Bayani, T. Hide, R.M. Henkelman, M.D. Cusimano, P.B. Dirks, Identification of human brain tumour initiating cells, Nature 432 (2004) 396–401.

[5] R. Galli, E. Binda, U. Orfanelli, B. Cipelletti, A. Gritti, S. De Vitis, R. Fiocco, C. Foroni, F. Dimeco, A. Vescovi, Isolation and characterization of tumorigenic, stem-like neural precursors from human glioblastoma, Cancer Res. 64 (2004) 7011–7021.

[6] X. Yuan, J. Curtin, Y. Xiong, G. Liu, S. Waschsmann-Hogiu, D.L. Farkas, K.L. Black, J.S. Yu, Isolation of cancer stem cells from adult glioblastoma multiforme, Oncogene 23 (2004) 9392–9400.

[7] P. van der Valk, J. Lindeman, W. Kamphorst, Growth factor profiles of human gliomas. Do non-tumour cells contribute to tumour growth in glioma? Ann. Oncol. 8 (1997) 1023–1029.

[8] Y.H. Zhou, F. Tan, K.R. Hess, W.K. Yung, The expression of Pax6, PTEN, vascular endothelial growth factor, and epidermal growth factor receptor in gliomas: Relationship to tumor grade and survival, Clin. Cancer Res. 15 (2003) 3369–3375.

[9] L. Bello, V. Lucini, F. Costa, M. Pluderi, C. Giussani, F. Acerbi, G. Carrabba, M. Pannacci, D. Caronzolo, S. Grosso, S. Shinkaruk, F. Colleoni, X. Canron, G. Tomei, G. Deleris, A. Bikfalvi, Combinatorial administration of molecules that simultaneously inhibit angiogenesis and invasion leads to increased therapeutic efficacy in mouse models of malignant glioma, Clin. Cancer Res. 10 (2004) 4527–4537.

[10] A. Sawano, T. Takahashi, S. Yamaguchi, M. Aonuma, M. Shibuya, Flt-1 but not KDR/Flk-1 tyrosine kinase is a receptor for placenta growth factor, which is related to vascular endothelial growth factor, Cell Growth Differ. 7 (1996) 213–221.

[11] T. Nabekura, M. Otsu, T. Nagasawa, H. Nakauchi, M. Onodera, Potent vaccine therapy with dendritic cells genetically modified by the gene-silencing-resistant retroviral vector GCDNsap, Mol. Ther. 13 (2006) 301–309.
[12] A. Suzuki, K. Obi, T. Urabe, H. Hayakawa, M. Yamada, S. Kaneko, M. Onodera, Y. Mizuno, H. Mochizuki, Feasibility of ex vivo gene therapy for neurological disorders using the new retroviral vector GCDNsap packaged in the vesicular stomatitis virus G protein, J. Neurochem. 82 (2002) 953–960.
[13] M. Yamada, M. Onodera, Y. Mizuno, H. Mochizuki, Neurogenesis in olfactory bulb identified by retroviral labeling in normal and 1-methyl-4-phenyl-1,2,3,6-tetrahydropyridine-treated adult mice, Neuroscience 124 (2004) 173–181.
[14] J.C. Gollmer, A. Ladoux, J. Gioanni, P. Paquis, A. Dubreuil, M. Chatel, C. Frelin, Expression of vascular endothelial growth factor-b in human astrocytoma, Neuro-Oncology 2 (2000) 80–86.
[15] S. Ergün, N. Kiliç, W. Fiedler, A.K. Mukhopadhyay, Vascular endothelial growth factor and its receptors in normal human testicular tissue, Mol. Cell Endocrinol. 131 (1997) 9–20.
[16] S.Y. Cheng, M. Nagane, H.S. Huang, W.K. Cavenee, Intracerebral tumor-associated hemorrhage caused by overexpression of the vascular endothelial growth factor isoforms VEGF121 and VEGF165 but not VEGF189, Proc. Natl. Acad. Sci. USA 94 (1997) 12081–12087.
[17] P. Kleihues, D.N. Louis, B.W. Scheithauer, L.B. Rorke, G. Reifenberger, P.C. Burger, W.K. Cavenee, The WHO classification of tumors of the nervous system, J. Neuropathol. Exp. Neurol. 61 (2002) 215–225.
[18] T. Reya, S.J. Morrison, M.F. Clarke, I.L. Weissman, Stem cells, cancer, and cancer stem cells, Nature 414 (2001) 105–111.
[19] R. Pardal, M.F. Clarke, S.J. Morrison, Applying the principles of stem cell biology to cancer, Nat. Rev. Cancer 3 (2003) 895–902.
[20] A.E. Wurmser, T.D. Palmer, F.H. Gage, Cellular interactions in the stem cell niche, Science 304 (2004) 1253–1254.
[21] N. Sanai, A. Alvarez-Buylla, M.S. Berger, Neural stem cells and the origin of gliomas, N. Engl. J. Med. 353 (2005) 811–822.
[22] Q. Shen, S.K. Goderie, L. Jin, N. Karanth, Y. Sun, N. Abramova, P. Vincent, K. Pumiglia, S. Temple, Endothelial cells stimulate self-renewal and expand neurogenesis of neural stem cells, Science 304 (2004) 1253–1255.
[23] S. Bao, Q. Wu, S. Sathornsumetee, Y. Hao, Z. Li, A.B. Hjelmeland, Q. Shi, R.E. McLendon, D.D. Bigner, J.N. Rich, Stem cell-like glioma cells promote tumor angiogenesis through vascular endothelial growth factor, Cancer Res. 66 (2006) 7843–7848.
[24] M.F. Clarke, M. Fuller, Stem cells and cancer: Two faces of Eve, Cell 124 (2006) 1111–1115.
[25] J.L. Lasky, M.L. Liau, Targeting stem cells in brain tumors, Technol. Cancer Treat. 3 (2006) 251–260.

Journal of Neuroscience Research 85:1704–1712 (2007)

Postnatal Neurogenesis in Hippocampal Slice Cultures: Early In Vitro Labeling of Neural Precursor Cells Leads to Efficient Neuronal Production

Takashi Namba,[1,2] Hideki Mochizuki,[3,4] Masafumi Onodera,[5] Hideo Namiki,[2] and Tatsunori Seki[1]*

[1]Department of Anatomy, Juntendo University School of Medicine, Tokyo, Japan
[2]Major in Integrative Bioscience and Biomedical Engineering, School of Science and Engineering, Waseda University, Tokyo, Japan
[3]Department of Neurology, Juntendo University School of Medicine, Tokyo, Japan
[4]Research Institute for Diseases of Old Ages, Juntendo University School of Medicine, Tokyo, Japan
[5]Department of Hematology, Institute of Clinical Medicine, University of Tsukuba, Tsukuba, Japan

Neurogenesis continues throughout life in the hippocampus. To study postnatal neurogenesis in vitro, hippocampal slices from rats on postnatal day 5 (P5) were cultured on a porous membrane for 14 or 21 days. In the initial experiments, precursor cells were labeled with bromodeoxyuridine (BrdU) after 7 days in culture because hippocampal slices are generally used in experiments after 1–2 weeks in culture. Fourteen days after labeling, however, only about 10% of BrdU-labeled cells expressed neuronal markers, although in living rats, about 80% of cells labeled with BrdU on P5 had become neurons by P19. Next, rats were injected with BrdU 30 min before culture, after which hippocampal slices were cultured for 14 days to examine the capacity of in vivo–labeled neural precursors to differentiate into neurons in vitro. In this case, more than two-thirds of BrdU-labeled cells expressed neuronal markers, such as Hu, NeuN, and PSA-NCAM. Furthermore, precursor cells underwent early in vitro labeling by incubation with BrdU or a modified retrovirus vector carrying EGFP for 30 min from the beginning of the culture. This procedure resulted in a similar high rate of neuronal differentiation and normal development into granule cells. In addition, time-lapse imaging with retrovirus-EGFP revealed migration of neural precursors from the hilus to the granule cell layer. These results indicate that in vivo– and early in vitro–labeled cultures are readily available ex vivo models for studying postnatal neurogenesis and suggest that the capacity of neural precursors to differentiate into neurons is reduced during the culture period.

Key words: hippocampus; dentate gyrus; PSA-NCAM; migration; differentiation

Neurogenesis in the hippocampal dentate gyrus continues from the late embryonic stage to the adult stage in various vertebrates including humans (Altman and Das, 1965; Seki and Arai, 1993, 1995; Kuhn et al., 1996; Eriksson et al., 1998). Newly generated neurons are functionally incorporated into preexisting hippocampal circuits under the influence of hippocampal activities (van Praag et al., 2002; Tozuka et al., 2005; Tashiro et al., 2006). Because the dendrites and axons of the newly generated neurons form a huge number of synapses that could involve hippocampal plasticity, much attention has been paid to the relationship between adult neurogenesis and learning (Gould et al., 1999; Schmidt-Hieber et al., 2004). In addition, the fact that adult neurogenesis is modulated by seizures, ischemia, stress, and antidepressants has increased the number of clinical studies on adult neurogenesis (Gould et al., 1997; Parent et al., 1997; Liu et al., 1998; Malberg et al., 2000). However, most of these studies have been performed in vivo, and in vitro studies have been mainly confined to those using neurosphere or dispersed-cell cultures (Palmer et al., 1997; Seaberg and van der Kooy, 2002).

Organotypic slice cultures of the hippocampus are a popular ex vivo model and have several advantages for investigating the physiology, pharmacology, and pathology of hippocampal formation (Stoppini et al., 1991; Gahwiler et al., 1997; Sakaguchi et al., 1997). Cultured hippocampal slices maintain normal tissue organization and physiological

Contract grant sponsor: Japan Society for the Promotion of Science; Contract grant number: Grant-in-Aid for Scientific Research 17500238; Contract grant sponsor: High Technology Research Center Grant from the Japanese Ministry of Education, Culture, Sports and Science.

*Correspondence to: Tatsunori Seki, Department of Anatomy, Juntendo University School of Medicine, 2-1-1 Hongo, Bunkyo, Tokyo 113-8421, Japan. E-mail: tseki@med.juntendo.ac.jp

Received 31 October 2006; Revised 26 December 2006; Accepted 28 January 2007

Published online 23 April 2007 in Wiley InterScience (www.interscience.wiley.com). DOI: 10.1002/jnr.21295

membrane properties (Stoppini et al., 1991; Okada et al., 1995; Gahwiler et al., 1997) and can be directly observed under a fluorescent microscope or confocal laser-scanning microscope together with live cell labeling techniques. Furthermore, that postnatal neurogenesis requires microenvironments surrounding precursors (Palmer et al., 2000; Seki, 2002, 2003) suggests that a slice culture containing various neural and nonneural elements is a more suitable ex vivo model for postnatal neurogenesis than is a neurosphere culture. However, application of hippocampal organotypic slice cultures for postnatal neurogenesis is relatively rare (Kamada et al., 2004; Raineteau et al., 2004; Laskowski et al., 2005; Poulsen et al., 2005). Furthermore, neurogenesis in organotypic cultures has not been precisely assessed by comparison with in vivo neurogenesis of age-matched rats.

We recently reported the details of the developmental process of newly generated cells in the postnatal hippocampus (Namba et al., 2005). In the present study, we analyzed in vitro neurogenesis in an organotypic hippocampal slice culture on the basis of previous and present in vivo data. As a consequence, we found a useful labeling method for investigating neural development of neural precursor cells to allow efficient neuronal production similar to that in in vivo postnatal neurogenesis.

MATERIALS AND METHODS

All animal treatments were approved by the Institutional Animal Care and Use Committee at Juntendo University.

Slice Culture and Tissue Processing

Hippocampal slices were prepared from postnatal day 5 (P5) Wistar rats and cultured according to the standard interface method with several modifications (Stoppini et al., 1991; Sakaguchi et al., 1997; Kamada et al., 2004). Rats were briefly anesthetized with diethyl ether and then deeply anesthetized on ice. Their heads were cut and their brains removed. The hippocampi were dissected in minimum essential medium (MEM; Invitrogen, Carlsbad, CA) supplemented with 25 mM HEPES (Sigma, St. Louis, MO). Whole hippocampi were sliced into 350-μm-thick slices using a McIlwain tissue chopper (Mickle Laboratory Engineering, Guildford, Surrey, UK). The slices were randomly chosen from the hippocampus except for regions near the septal and temporal poles and transferred onto a porous membrane (Millicell-CM PICM03050; Millipore, Billerica, MA) and maintained in an incubator at 34°C with a 5% CO_2-enriched atmosphere. The culture medium was 50% MEM (Invitrogen), 25% heat-inactivated horse serum (Invitrogen), and 25% Hank's balanced salt solution (Invitrogen) supplemented with penicillin-streptomycin-glutamine (Invitrogen) and glucose (final concentration, 6.5 mg/mL). The medium was changed twice a week. Two weeks after bromodeoxyuridine or retrovirus (RV) treatment, the slices were fixed by 4% paraformaldehyde in 0.1M phosphate buffer (PB), pH 7.4, for 8 hr at 4°C. The fixed slices were embedded in 5% agar, washed 3 times with PBS, and immersed in 10% and then 20% sucrose in PBS over 2 days. Next, the slices were embedded in an OTC compound, frozen in liquid nitrogen, and stored at −80°C. The slices were sectioned with a cryostat into 30-μm-thick sections.

5-Bromo-2-deoxyuridine and Retrovirus Treatment

Newly generated cells were labeled by three methods: (1) intraperitoneal injection of 5-bromo-2-deoxyuridine (BrdU; Sigma) dissolved in 0.9% NaCl (50 mg/kg body weight) into P5 rats 30 min before slice preparation, (2) incubation with 1 μM BrdU-containing culture medium for 30 min from the beginning of culture, or (3) incubation with 1 μM BrdU-containing culture medium for 1 day after 7 days in vitro (DIV). To visualize the newly generated cells, we used our modified retrovirus vector, GCDNsap-EGFP. Details of the construction and titer of this vector were described previously (Suzuki et al., 2002). Drops of GCDNsap-EGFP retrovirus solution were put on the cultured slices at the beginning of the culture (0.5 μL per slice). For time-lapse imaging, a retrovirus vector (0.5 μL) was stereotactically injected into the hilus of P5 rats (posterior = 1.2 mm from bregma, lateral = 2.1 mm, ventral = 2 mm), as described previously (Namba et al., 2005).

Time Lapse Imaging

Three days after the retroviral injection (P8), 350-μm-thick hippocampal slices were cultured as described above. Time-lapse recording was performed manually using an inverted confocal laser-scanning microscope (LSM510META; Zeiss, Germany). To follow the movements of the labeled cells, stacks of images were collected in the z plane every day using a 20× objective. Between time points, the slices were kept in an incubator at 37°C and 5% CO_2.

In Vivo Experiments

Rats on postnatal day 5 (P5) were given an intraperitoneal injection of BrdU (Sigma) dissolved in 0.9% NaCl (50 mg/kg body weight) or a stereotactic injection into the dentate gyrus of the hippocampus of 0.5 μL of GCDNsap-EGFP retrovirus (Suzuki et al., 2002; Tanaka et al., 2004; Namba et al., 2005) as described above. Fourteen days (P19) after the BrdU or RV injection, the rats were perfused and processed as described previously (Namba et al., 2005). The tissues were thawed and washed in PBS, embedded in 5% agarose in PBS, and sectioned by a vibratome into 50-μm-thick sections.

Antibodies and Immunofluorescent Staining

The antibodies used in this work, their concentrations, and the vendors that supplied them are listed in Table I. The primary and secondary antibodies were diluted with PBS containing 1% bovine serum albumin (BSA). The sections of the hippocampal slices were washed with PBS. All subsequent incubations were carried out with free-floating sections in 10-mL vials using a rotator. Each of the following steps was followed by washing with PBS. To stain PSA-NCAM, the sections were pretreated with 100% methanol. They were incubated with various combinations of the primary antibodies diluted in PBS containing 1% BSA at 4°C for 24 hr and then incubated at room temperature for 1–2 hr with a mixture of

TABLE I. Antibodies

Marker	Species, isotype	Label	Working dilution	Vendor
Primary antibodies				
BrdU	Rat IgG	none	1:200	ImmunologicalsDirect.com, UK
GFP	Mouse IgG	none	1:400	Sigma, Mo, USA
GFP	Rabbit IgG	none	1:200	Gift from Dr. N. Tamamaki*
GFP	Rat IgG	none	1:400	Nakalai Tesque, Japan
Iba-1	Rabbit IgG	none	1:1000	Wako, Japan
Hu	Human IgG	none	1:2000	Gift from Dr. HJ. Okano**
Hu	Mouse IgG	none	1:100	Molecular Probes, OR, USA
Ki67	Mouse IgG	none	1:100	Novocastra Laboratories, UK
NeuN	Mouse IgG	none	1:200	Chemicon International, CA, USA
PSA-NCAM (12E3)	Mouse IgM	none	1:500	Raised in our laboratory***
RIP	Mouse IgG	none	1:20000	Chemicon International
S100β	Mouse IgG	none	1:2000	Sigma
S100β	Rabbit IgG	none	1:5000	Swant, Switzerland
Secondary antibodies				
Anti-human IgG	Donkey IgG	Cy3	1:200	Jackson, PA, USA
Anti-mouse IgG	Donkey IgG	Cy2	1:200	Jackson
Anti-mouse IgG	Donkey IgG	Cy5	1:200	Jackson
Anti-mouse IgG(Fcγ)	Goat IgG	Cy5	1:200	Jackson
Anti-mouse IgM	Donkey IgG	Cy2	1:200	Jackson
Anti-rabbit IgG	Donkey IgG	Cy2	1:200	Jackson
Anti-rabbit IgG	Donkey IgG	Cy5	1:200	Jackson
Anti-rabbit IgG	Donkey IgG	FITC	1:200	Jackson
Anti-rat IgG	Donkey IgG	Cy2	1:200	Jackson
Anti-rat IgG	Donkey IgG	Cy3	1:200	Jackson

*Tamamaki et al., 2000;
**Okano and Darnell, 1997;
***Seki and Arai, 1991.

secondary antibodies. For BrdU analysis, the sections were subsequently treated with 2N HCl at 37°C for 35 min and neutralized with 0.1M borate buffer (pH 8.5). Next, they were incubated with rat monoclonal anti-BrdU antibody at 4°C overnight and then with Cy3-conjugated anti-rat IgG. Finally, the specimens were mounted on glass slides. The samples were viewed through a Zeiss confocal laser-scanning microscope (LSM510 and LSM510 META) with 20×, 40×, 63×, and 100× objectives. The images were corrected for brightness and contrast using a Zeiss LSM image Browser, Adobe Illustrator 9.0, and Adobe Photoshop 7.0. When the primary antibodies were omitted from the immunofluorescent staining, no immunoreactivity was detected.

Cell Counting

To determine the number of BrdU-, GFP-, Hu-, NeuN-, PSA-NCAM-, and S100β-positive cells in the granule cell layer (GCL) including the subgranular zone and the hilum of cultured slices, 1 of 5 sections per cultured slice was used, and each experimental group consisted of 7–21 cultured slices from 3 or 4 independent rats. An average of 5 sections per rat was used for the in vivo analysis, and each experimental group consisted of 3–5 rats. Adjacent sections were not used for cell counting to avoid double counting. All counting was performed under a confocal laser-scanning microscope using a 40×objective for stacks of 5 optical sections. Data were analyzed statistically using one-way analysis of variance followed by the Scheffé post hoc *F* test. All values are given as means ± SEMs.

Morphological Analysis

To analyze the morphological characteristics of the GFP+/Hu+ cells, a Z series of images was obtained under the Zeiss confocal laser-scanning microscope (LSM510 and LSM510 META) using a 40× objective. The number of dendritic branching points and dendrite length were measured three-dimensionally using Imaris 4 (Zeiss) and the Imaris Measurement Pro (Zeiss). Data were analyzed statistically using one-way analysis of variance followed by the Scheffé post hoc *F* test. All values are given as means ± SEMs.

RESULTS

Late In Vitro–Labeled Cultures

Because cultured slices are generally used in experiments after 1–2 weeks in culture (Okada et al., 1995), in the initial experiments hippocampal slices from P5–P6 rats were treated with BrdU from DIV 7 to DIV 8 and fixed 14 days after BrdU treatment (DIV 21; Fig. 1A). Triple immunostaining revealed that a small proportion of BrdU-positive (BrdU+) cells expressed a neuronal marker, Hu (9.40% ± 2.1%), and that a large proportion were S100β-positve (16.0% ± 1.8%) and double-negative cells (74.6% ± 2.9%, n = 8 slices from 3 rats; Figs. 2A, 3A). Most of the double-negative cells should have been microglial cells because approximately half the BrdU-labeled cells expressed the microglial marker Iba-1 (data not shown). The numbers of BrdU/RIP-double-